TURBINE DESIGN TO MITIGATE FORCING

John P. Clark
Principal Engineer
Turbine Branch, Turbine Engine Division
Propulsion Directorate, Air Force Research Laboratory
Building 18, Room 136D
1950 5th St., WPAFB, OH 45433
USA
john.clark.38@us.af.mil

The ability to predict accurately the levels of unsteady forcing on turbine blades is critical to avoid high-cycle fatigue failures. Further, a demonstrated ability to make accurate predictions leads to the possibility of controlling levels of unsteadiness through aerodynamic design. There are several desiderata to achieve designs that experience reduced forcing functions. First, and quite simply, any such design is by definition grounded in the basic physics of the flow. Second, confidence in the fidelity of the design-level analyses used to predict the relevant flow physics is critical. This in turns means that design analyses are as well validated as possible and that both the viscous and geometric modeling of the turbine is appropriate to the problem. Additionally, it is critical that proper periodicity of the predicted flowfield is achieved during design-level analyses. An ability to judge this is in turn dependent on an understanding of basic concepts in digital signal processing that are also essential to the accurate calculation of unsteady forces on airfoils. Here, a method to assess the convergence of periodic flowfields is presented with reference to an experimental turbine designed at the Air Force Research Laboratory. Then, the physics of the flowfield in this turbine that gives rise to unsteady interactions is discussed with reference to available code-validation data. Finally, several design techniques are considered either to reduce the magnitude or alter the phase of unsteady interactions within the turbine in order to mitigate forcing. These include the shaping of both the rotating and stationary airfoil profiles as well as a novel flow-control method that involves steady blowing from the pressure side of the downstream stationary airfoil row. In addition, the effects of downstream vane asymmetric spacing and vane-to-vane clocking are also assessed. While at present the application of these concepts to the turbine in question is strictly analytical, experimental validation of many of these methods to reduce unsteadiness is now underway in a full-scale rotating, transonic turbine experiment at AFRL.

1. Introduction

Periodic unsteadiness is inherent to flows in gas turbine engines, and in consequence very many studies have been devoted to the understanding of unsteady flows in turbomachines over a large number of years. There are seminal investigations that have delved into the theoretical (e.g. Tyler and Sofrin [1] and Rangwalla and Rai [2]), experimental (e.g. Dring et al. [3], Dunn and Haldeman [4]), and computational (e.g. Rai [5], Giles [6]) aspects of rotor-stator interactions. In addition, reviews of the state of the art are available (Greitzer et al. [7] and Sharma et al. [8]) as well as more general introductions to the subject (e.g. Paniagua and Denos [9]). In recent reviews of turbine durability and aerodynamic predictive tools, respectively, Dunn [10] and Adamczyk [11] have made the point that the fidelity of flowfield predictions has increased accordingly as the state-of-the-art for CFD calculations in the gas turbine industry has progressed. The increased predictive capability of turbine design codes has allowed for better turbomachinery designs and improved understanding of the physical mechanisms that are prevalent in turbomachines, especially when used to complement experimental findings.

Greitzer et al. [7] discussed time-varying flowfields and the aero-mechanical excitation that can result from such unsteadiness. The authors stated that, in general, levels of unsteady forcing that give rise to High-Cycle Fatigue (HCF) problems during engine development had to that time not been well predicted. They described the current design process for turbine blades as one of resonant-avoidance. Typically, modern structural-analysis tools are used to predict the natural frequencies of vibratory modes with acceptable accuracy, and these are plotted versus wheel speed on a Campbell diagram along with the frequencies of expected stress drivers in the system. Fig. 1.1 is an example diagram for a stainless-steel high turbine blade tested in a code validation study. As an example, a design practice might encompass ensuring that there are no expected resonances for any of the lower-order modes in the operating range of the machine (a turbine rig in the case of Fig. 1.1). Sometimes, however, successful execution of this design practice is not feasible. So, Greitzer et al. [7] concluded that blade forced-response and the high-cycle fatigue failures that can result from it were of sufficient interest to the gas-turbine community that "…a decrease in the level of empiricism [in that area] would be of significant value in the engine development process." Practically, this meant that faster and more accurate predictions of the magnitudes of unsteady forcing functions were required.

Toward that end, developments in predictive methods such as multi-grid techniques and implicit dual time-stepping, coupled with parallelization of codes (Ni [12]) have made it possible for designers to execute 3-D, unsteady Navier-Stokes analyses routinely during the design cycle. So, designers can now routinely predict periodic-unsteady forcing functions and the calculation of resonant stresses in multi-row turbomachinery is now widespread in the industry [13-19]. Consequently, it is now possible to make design changes as necessary based

on the outcome of such calculations. Also, short-duration experimental facilities that allow for accurate modeling of modern gas-turbine flowfields (e.g. Jones et al. [20] and Dunn et al. [21]) are often used to assess the capabilities of state-of-the-art codes. In particular, the abilities of the codes to predict both the time-averaged and time-resolved pressure loadings on transonic airfoils were investigated by Rao et al. [22], Busby et al. [23], Hilditch et al. [24], and many others [25-28]. This has even been extended to include an assessment of the structural response due to forcing by Kielb et al. [29] and Hennings and Elliot [30] as well as both the aerodynamic and mechanical damping Kielb and Abhari [31]. In addition, design-optimization systems have been used effectively in conjunction with steady-state flow solvers to reduce the strength of shock waves emanating from transonic turbine blades and decrease interaction losses as well as, presumably, resonant stresses by Jennions and Adamczyk [32].
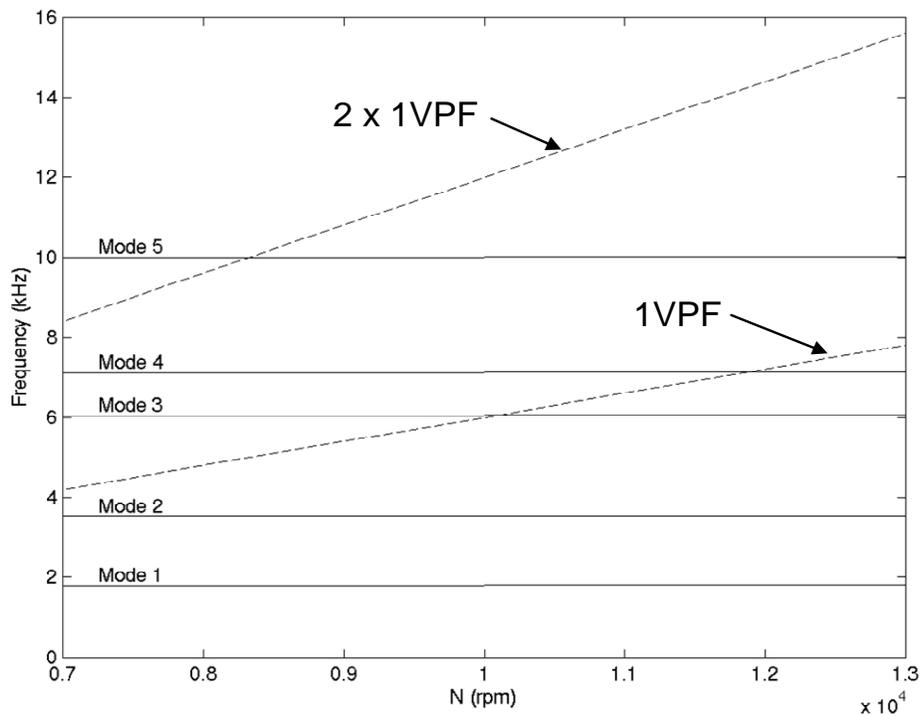
Fig. 1.1   Example Campbell diagram for a turbine blade

Turbomachinery designers often employ both steady-state and time-resolved predictive tools during the development of new engines. The major difference between the methods is the numerical treatment of the inter-row boundary. For steady-state turbomachinery simulations, common methodologies include the average-passage formulation of Adamczyk [11] and the mixing plane as employed in the Ni code [12, 33-35]. In the latter, the flow from an upstream blade row is circumferentially averaged and then the flow properties are passed into the downstream row as a radial profile. For many situations the difference between the steady-state flowfield and the time-average of an unsteady solution is minor. However, it is the time-resolved information that is often of most critical importance to the designer, as in the case of predicting resonant stresses in the machine.

Resonant stresses can arise as a consequence of the interaction between a turbine blade and airfoil wakes, potential fields, and/or shocks that can travel downstream and/or upstream through the engine. Turbine airfoil surfaces constantly encounter fluctuating flowfields induced by such flow structures. These can manifest as pressure fluctuations that impart time-varying forces that generate cyclic rotor vibratory stresses that can in turn reduce the life of the airfoil. Design methodologies are constantly being improved to predict these airfoil vibratory stresses, and such computations are now performed in the design cycle at many companies [13-19, and 36]. Additionally, design strategies to increase aerodynamic performance and turbine durability can have a detrimental effect on the fatigue life of turbine components. One performance-enhancing design feature involves the intentional shifting of circumferential position between successive blade and/or vane rows [37-40]. Known as airfoil clocking, this relative difference in circumferential position is used to control the location of upstream airfoil wakes as they propagate through downstream airfoil passages in order to achieve a performance benefit in terms of increased efficiency. However, it is possible that the relative phase of an upstream-propagating potential field and downstream-propagating vortical disturbances could act to increase the unsteady load on a turbine blade that is located between clocked vane rows. In terms of turbine durability enhancements, sometimes fuel nozzles and turbine nozzle guide vanes are also clocked in an effort to reduce the heat load to downstream components [41-44]. Although there is no effect on the potential field inside the vane row [45], there is usually a variation in the unsteady pressure load on the turbine blades downstream of the vane.

2. Assessment of Periodic-Flow Convergence and Considerations from Digital Signal Processing

Predictions of time-resolved flowfields are now commonplace within the gas-turbine industry, and the results of such simulations are now sometimes used to make design decisions during the development of new products. Hence, it is necessary for analysts to have a robust method to determine the level of convergence in design predictions. In this section, a method to determine the level of convergence in a predicted flowfield that is characterized by periodic-unsteadiness is presented. The method relies on fundamental concepts from digital signal processing that are themselves of great utility to the turbine engineer that is designing with unsteady aerodynamics in mind. These concepts include the discrete Fourier transform, cross-correlation, and Parseval's theorem. Often in predictions of vane-blade interaction in turbomachines, the period of the unsteady fluctuations is expected. In this method, the development of time-mean quantities, Fourier components (both magnitude and phase), cross-correlations, and integrated signal power are tracked at locations of interest from one period to the next as the solution progresses. Each of these separate quantities yields some relative measure of convergence that is subsequently processed to form a fuzzy set. Thus the overall level of convergence in the solution is given by the intersection of these sets. Examples of the

application of this technique to predictions of vane/blade interaction using two separate solvers are given. It is shown that the method yields a robust determination of convergence. Also, the results of the technique can guide further analysis and/or post-processing of the flowfield. Finally, the method is useful for the detection of inherent unsteadiness in the flow, and so it can be used to prevent instances of non-synchronous vibration (NSV).

2.1 The Need for Rigorous Assessment of Periodic-Convergence

There are well established means for determining the accuracy of CFD simulations with respect to grid- and time-step convergence [46, 47]. This has led to policy statements from the engineering societies with respect to code verification and validation in general [48] and numerical accuracy in particular [49]. Of interest here is "iterative convergence." The policy statement from the ASME *Journal of Fluids Engineering* [49] states that, "stopping criteria for iterative calculations must be precisely explained, [and] estimates must be given for the corresponding convergence error." Iterative convergence criteria for steady-state simulations are well established: convergence is typically measured by tracking the iteration-to-iteration change of one or more flowfield quantities and looking for this value either to drop below a minimum threshold or to reach a zero slope. In an unsteady CFD simulation, the time-periodic nature of the flowfield precludes such a measure of convergence. So, some other technique is required.

In the gas-turbine industry designers often make simple qualitative judgments as to periodicity of the flow, and this is seldom based on interrogation of more than a few signals. Further, in most publications, discussion of unsteady convergence is cursory at best. One exception is due to Laumert et al. [50], who defined convergence of their unsteady simulation as occurring when the maximum deviation in static pressure between two periodic intervals was less than 0.1% over the airfoil surface at midspan. More recently, Ahmed and Barber [51] defined unsteady convergence in terms of time-varying Fast Fourier Transform (FFT) magnitudes calculated as the solution progresses. As time-resolved flowfield predictions become an ever increasing part of physics-based design systems the need for quantitative measures of iterative convergence becomes critical. This is particularly true when time-resolved CFD is used during detailed design where both rapid turn-around time and predictive accuracy are critical.

Design-optimization systems are becoming more and more prevalent within the industry [52-54], and using time-accurate CFD within such a system necessarily requires quantitative convergence monitoring. The computational time required to obtain a valid solution when considering a given perturbation of a set of design parameters is critical to the feasibility of an optimization study. Without a converged solution from which to extract one or more parameters used in an objective (or fitness) function, it is not possible to determine a correct relationship between the perturbed design parameters and the design objective. One is left

with little choice but to set each optimization perturbation to run a high number of iterations to ensure convergence. Consequently, the potential savings in the wall-clock time required to achieve a given objective is significant if a time-resolved convergence criterion is available.

A robust, quantitative process for assessing the level of convergence of a time-accurate simulation is required. Ideally, the method should consist of calculations that both track the progress of the simulation and allow for the detection of inherent unsteadiness in the flowfield. Here a measure of time-periodic convergence is defined and applied to a pair of unsteady simulations relevant to modern gas-turbine design. Again, application of the technique ensures the effective usage of time-accurate analyses during traditional design exercises to predict unsteady forcing, and it enables effective unsteady optimization.

2.2   Qualities of an Unsteady Convergence Criterion

Often in flowfield predictions in turbomachines, the period of the most significant unsteady fluctuations is expected from the circumferential interval modeled and the known wheel speed. During the execution of the time-accurate simulation, one can monitor various aspects of the flowfield at discrete intervals equal to some multiple of the computational time step. Then, one can calculate time-mean and time-resolved quantities of interest: these may include but are not limited to the mass flow rates through domain inlet and exit boundaries, total pressures and temperatures (e.g. to obtain aero-performance), and static pressures on airfoil surfaces (e.g. to calculate resonant stresses). The collection of these quantities over the iteration history of the solution provides a set of discrete, time-varying signals which one can manipulate using standard signal processing techniques to quantify periodic convergence. Here, we describe a set of signal processing operations that were selected carefully for this purpose on the basis of their relevance to both the design process in general and the case of periodic unsteadiness in particular. One can find more details on the techniques in the text by Ifeachor and Jervis [55] and in [56].

As mentioned above, designers primarily perform unsteady simulations either to determine the effect of design changes on the time-mean characteristics of the machine (e.g. aero-performance or heat load) or to estimate resonant stresses on the airfoils. So, the development of both time-mean and time-resolved quantities is important for unsteady convergence monitoring. It is straightforward to track the former over periodic intervals, but the latter requires some consideration. Resonant stress analyses are typically performed at discrete engine orders consistent with the Campbell diagram of the airfoil row. Such calculations require accurate information on the unsteady forces on the airfoil row, and this includes both magnitude and phase information at the frequencies of interest. These frequencies are driven by the airfoil counts in the machine where both the fundamental frequencies and a number of harmonics may be important. So, it is necessary at a minimum to track the development of the magnitude and phase of relevant frequencies from periodic interval to periodic interval as

well as time-mean quantities. Further, Jocker and Fransson [57] have clearly demonstrated the importance of the phase of periodic fluctuations in determining the level of excitation of a vibrating airfoil.

An effective convergence criterion for unsteady flows also allows for the possibility of inherent unsteadiness (i.e. unexpected flow physics that can affect airfoil life) existing in a flowfield. This often occurs in turbomachinery as a consequence of vortex shedding at the trailing edge of the airfoil. Such shedding can occur whether or not a significant separation zone exists on the airfoil suction surface, and the frequency is dictated by the relevant Strouhal number of the flow over the airfoil. Fortunately, two other signal analysis measures, cross-correlation and the power spectral density, are useful under such circumstances.

One can cross-correlate a time-varying signal determined over one expected periodic interval with the same signal calculated over the next period. The result is itself a repeating signal that should have the same period as that expected in the simulation. Further, the magnitude of the cross-correlation coefficient at zero lag is a direct measure of how alike the signal is over each of the pair of expected periodic intervals. If significant inherent unsteadiness exists in the flowfield, then the magnitude at zero lag can be significantly less than one, and the period of the cross-correlation coefficient can occur at a number of lags that is inconsistent with that expected in the simulation.

In signal processing Parseval's theorem states that the integral of the power spectral density over a defined range of frequencies is equal to the contribution of fluctuations on that interval to the overall mean square of the signal. Consequently, one can sum the power spectral densities over all significant frequencies expected in the simulation and compare that to the overall mean square. If the summed signal power is not a large fraction of the overall signal variance, then either inherent unsteadiness exists in the flowfield or a higher harmonic of the fundamental passing frequencies is more significant than expected. Of course, it is also possible to use the level of the power spectral density to determine the frequencies associated with the inherent unsteadiness and/or the higher harmonics, and one can then alter the execution of the unsteady simulation (and subsequent post-processing and resonant stress analysis) accordingly. This is often critical to avoid picket fencing and spectral leakage effects that can reduce the accuracy of predicted Fourier components of the signal [55], thus rendering resonant stress calculations inaccurate.

It is clear that all of the above measures are important for an assessment of unsteady convergence, and one can obtain a means for combining all the relevant information into a single measure from the field of fuzzy logic. Klir et al. [58] describe the process of "fuzzy decision making" that applies in situations such as these, and Clark and Yuan [59] have previously used the method to detect the edges of turbulent spots in a transitional flowfield consistent with a turbine blade. Further details regarding decision making in multi-valued

logic can be found in Zimmermann [60] and Klir and Yuan [61]. The process employed here is described below along with complete details of the convergence assessment method.

2.3 A Method for Unsteady Convergence Assessment

It is useful to describe the details of the current method with respect to example periodic-unsteady flowfields in turbomachines. One machine that is convenient for this purpose is the AFRL High Impact Technologies Research Turbine (HIT RT). An early design iteration of the turbine denoted here as HPT1, is described in detail by Johnson [62]. The geometry is a single-stage high-pressure turbine consistent with an engine cycle envisaged for 2020 and beyond. The vane and blade airfoil counts of HPT1 are 22 and 44, respectively. The turbine was analyzed via the 3D time-accurate Reynolds-Averaged Navier Stokes (RANS) solver of Dorney and Davis [63], which is itself a further development of the Rai code [5, 64].

The build 1 HIT RT geometry is shown in Fig. 2.1 as the full wheel of the machine, and the operating conditions of the present turbine simulation are listed in Table 2.1. Colorization of the non-slip surfaces in the figure is based on instantaneous static pressure. The wheel speed of HPT1 at conditions consistent with a short-duration rig experiment for design-system code validation in the AFRL Turbine Research Facility [65, 66] is 7050 rpm, and with $1/22^{nd}$ of the annulus modeled the expected periodicity occurs on an interval equal to approximately 0.387 ms. This time period corresponds to one vane-passing per blade or the passage of two blades per vane. At the time-step depicted in Fig. 2.2, the simulation had completed approximately 19 periodic cycles (vane passings), and the time-varying pressure at a location on the blade pressure side for the 2 subsequent cycles is plotted in Fig. 2.2a. While a surface static pressure on the blade pressure side is used in the present example, it is possible to use the method with any flow variable at any location of interest in the domain that is relevant to the design issue at hand.

Table 2.1 Operating conditions for a pair of example turbines.

	Re (1V,exit)	Vane M_{exit}	Blade M_{exit}
HPT1	2.4×10^6	0.82	1.40
HPT2	2.0×10^6	0.75	0.94

All signal-analysis operations required to apply the convergence-assessment method are illustrated in Fig. 2.2a-2.2e. Again, these are the calculation of the time-mean of the flow quantity over each periodic cycle, the Discrete Fourier Transform (DFT), the cross-correlation coefficient (CCF), and the power spectral density (PSD). In keeping with the nomenclature of [56] the time-mean of the static pressure over a single periodic cycle is

$$\overline{p} = \frac{1}{N} \sum_{n=0}^{N-1} p(n+1)$$

(2.1)
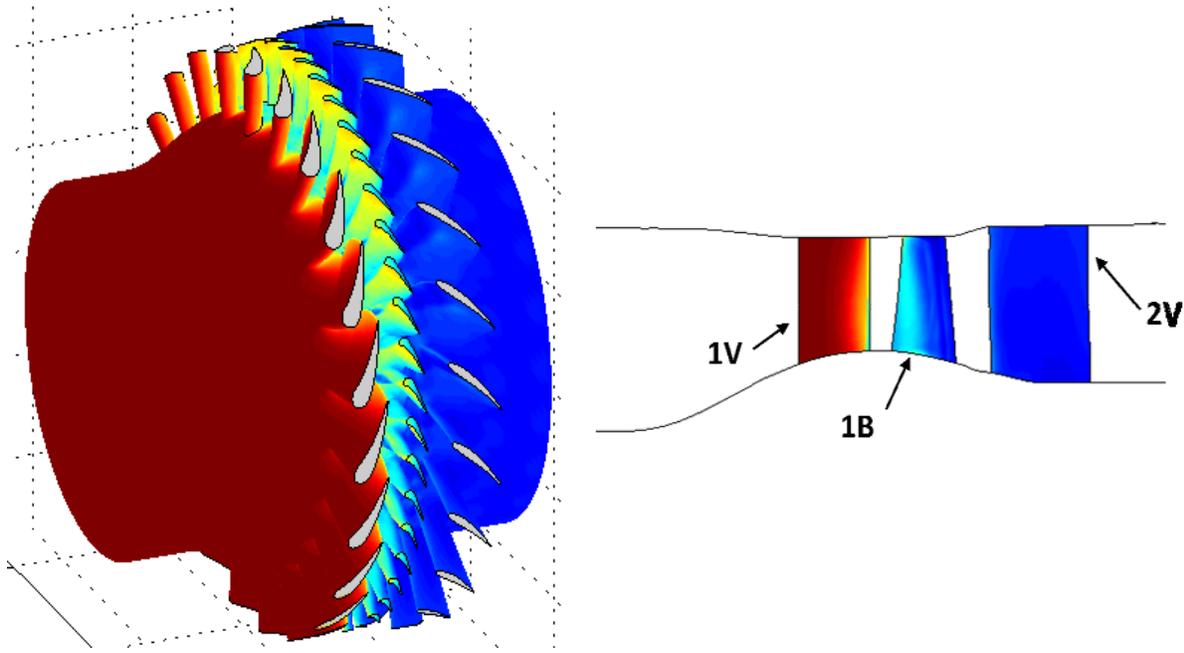
Fig. 2.1   The AFRL High Impact Technologies Research Turbine (HIT RT)

where N is the number of times steps per period and $p(n+1)$ is the static pressure calculated at an integer multiple, $n+1$, of the time step, Δt. In Fig. 2.2(a) the time-mean levels calculated over each of the two periodic cycles are plotted as well as the raw pressure trace. Complete convergence of the time-averaged signal is achieved when there is no difference in signal mean from one periodic interval to the next, and this is akin to steady-state convergence.

The Discrete Fourier Transform of the fluctuating pressure, p', evaluated at an integer multiple, $k+1$, of the signal sampling frequency, $\Delta f = (N \Delta t)^{-1}$ is given by

$$P(k+1) = \sum_{n=0}^{N-1} p'(n+1) e^{-i\frac{2\pi k n}{N}} \qquad (2.2)$$

where Fourier components are defined for values of k between 0 and N-1. Each Fourier component is a phasor, and the time-periodic fluctuation at a given multiple of the sampling frequency can be reconstructed by

$$p(t) = \text{Re}\left\{ A e^{i(\omega t + \phi)} \right\} = A \cos(\omega t + \phi) \qquad (2.3)$$

In Equation 2.3, A is the normalized DFT magnitude and Φ is the phase angle, given by
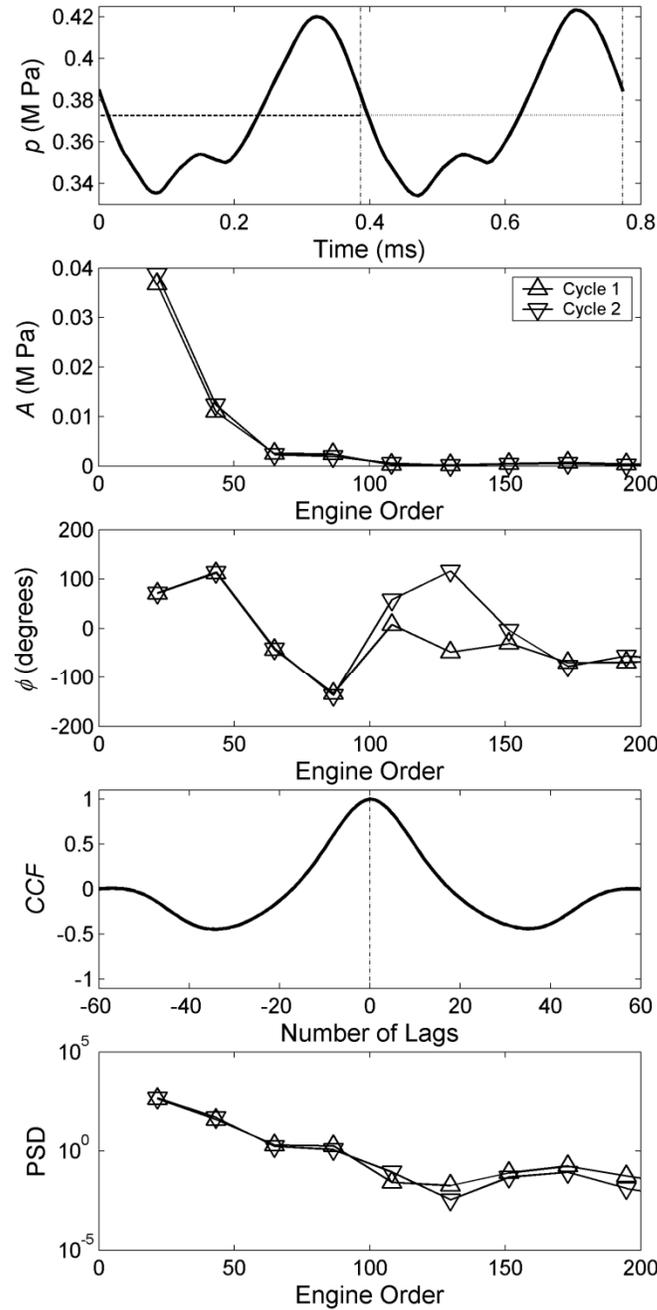
Fig. 2.2   An example of digital signal processing techniques used in the current method for HPT1: (a) time mean; (b) DFT magnitudes; (c) phase angles; (d) cross-correlation coefficients; and (e) power-spectral densities.

$$A = 2\left(\text{Re}^2 + \text{Im}^2\right)^{\frac{1}{2}} / N \quad ; \quad \phi = \tan^{-1}\left(\text{Im} / \text{Re}\right) \tag{2.4}$$

respectively. Also, ω is the circular frequency corresponding to the integer multiple of the sampling frequency, $2\pi\,\Delta f\,(k+1)$. DFT magnitudes and phase angles are plotted in Figs. 2.2(b) and 2.2(c), respectively for each of the periodic intervals plotted in Fig. 2.2(a). Convergence of the simulation at a given frequency is complete when there is neither a

change in magnitude nor a difference in phase between the DFT results for two consecutive periodic intervals at frequencies of interest to the designer.

The results of a cross-correlation of the signals from the two periodic cycles of Fig. 2.2(a) are plotted in Fig. 2.2(d). In the time domain the cross-correlation coefficient (*CCF*) is given by

$$CCF(L) = \frac{\frac{1}{N}\sum_{n=0}^{N-1} p'((n+1)+L)\,p'((n+1)+N)}{\frac{1}{N}\left[\sum_{n=0}^{N-1} p'^2\,(n+1)\ \ \sum_{n=0}^{N-1} p'^2\,((n+1)+N)\right]^{\frac{1}{2}}} \qquad (2.5)$$

The calculation at a given time lag, *L*, is accomplished first by multiplying the time-lag-shifted fluctuating pressure over the first interval by the fluctuating pressure signal for the second periodic interval, summing products, and then dividing by the number of samples per period. The result is then normalized by the product of the root-mean-square levels for the two signals. Complete convergence of the unsteady simulation yields a cross-correlation coefficient equal to 1 at zero lag. This implies that the signals from the first and second periodic intervals are exactly alike and that the expected period, *N*, is the true period of the signals.

The power spectral densities (PSD) of the signals from the two periodic intervals plotted in Fig. 2.2(a) are shown in Fig. 2.2(e). The PSD at a given multiple of the sampling frequency is defined as the product of the Fourier component at that frequency and its complex conjugate divided by the number of samples, *N*. Convergence of a time-resolved turbomachinery simulation occurs when a large fraction of the overall signal power occurs at frequencies of interest and when that portion of the mean square does not change from one periodic interval to the next.

It is useful to calculate a single parameter that can be used to gauge the level of convergence of the simulation, and multi-valued (i.e. fuzzy) logic provides a convenient means of accomplishing this objective [58]. One can use the calculated time-mean levels, DFT magnitudes and phase angles, cross-correlation coefficients at zero lag, and fraction of overall signal power at frequencies of interest to define a series of fuzzy sets that express various aspects of the degree of convergence. These fuzzy sets are as follows

$$f_M = 1 - \left| 1 - \frac{\overline{p}_2}{\overline{p}_1} \right| \qquad (2.6)$$

$$f_A = 1 - \left| 1 - \frac{A_2}{A_1} \right| \qquad (2.7)$$

$$f_\phi = 1 - \left| \frac{\phi_2 - \phi_1}{\pi} \right| \qquad (2.8)$$

$$f_S = \left| CCF(0) \right| \qquad (2.9)$$

$$f_P = \frac{\displaystyle\sum_{k_{\text{expected}}} PSD(k+1)}{\displaystyle\sum_{k=0}^{N-1} PSD(k+1)} \qquad (2.10)$$

where the subscripts 1 and 2 refer to the first and second cycles, respectively. Evaluation of Equations 2.6-2.10 give membership grades in fuzzy sets that describe consistent mean level, amplitude, phase angle, overall signal shape, and fractional signal power, respectively. The amplitude and phase membership grades of Equations 2.7 and 2.8 are calculated for each frequency of interest as defined, for example, by an airfoil Campbell diagram. The numerator in Equation 2.10 is a summation over all frequencies expected to produce significant signal power in the simulation. A level substantially less than 1 implies the presence of either inherent unsteadiness in the simulation or a significant signal level due to some higher harmonic of the expected fundamental frequencies. If the former is true, the inherent unsteadiness can dominate the signal, and the fuzzy set associated with consistent signal shape, f_S, typically has a value substantially less than one. Again, this would mean that DFT magnitudes and phase angles used to evaluate f_A and f_φ are suspect, and additional signal processing is required using the true period of the signals. Fortunately, this is given by the time lag associated with the maximum value of the cross-correlation function from Eq. 2.5.

The overall convergence level is then itself a fuzzy set defined as the intersection of the others, and this is in turn given by the standard fuzzy intersection [58].

$$f_C = f_M \cap f_A \cap f_\phi \cap f_S \cap f_P = \min(f_M, f_A, f_\phi, f_S, f_P) \qquad (2.11)$$

Here we define $f_C \geq 0.95$ for two consecutive cycles to be consistent with convergence of the periodic-unsteady flowfield. To continue this example, Equations 2.6-2.11 were evaluated for the signals plotted in Fig. 2.2, and the results are shown in Table 2.2. For this simulation, significant unsteadiness was expected to occur due to the fundamental vane-passing frequency (22E) as well as two harmonics of that frequency (44E and 66E). Note that more than 99% of the overall signal power is contained in the expected frequencies, so there is not any significant inherent unsteadiness evidenced in the signal. Also note that the signals are 99.9% correlated between the two periodic intervals, so the overall signal shape is very well converged. There is very little phase difference between cycles at the frequencies of interest, and the variation of amplitudes between cycles is greatest for the first harmonic of the fundamental. As a consequence, the overall convergence level of the simulation is 0.886, and this is dictated by the change in amplitude of that engine order (44E) from cycle to cycle.

Table 2.2 Results of the fuzzy-set convergence analysis as applied to the signals in Fig. 2.2.

Fuzzy Set	Membership Grade
f_M	0.999
f_A (22E)	0.947
f_ϕ (22E)	0.991
f_A (44E)	0.886
f_ϕ (44E)	0.990
f_A (66E)	0.933
f_ϕ (66E)	0.988
f_S	0.999
f_P	0.997
f_C	0.886

At this point, it is worth noting that the fuzzy sets f_M and f_S taken together are akin to the sort of information that an "expert user" of unsteady CFD employs to judge the convergence of a simulation. Such an expert would typically plot the time-variation of flowfield quantities for two or more periodic cycles and make a judgment as to how alike the DC and AC components of the signal are from one cycle to the next. In this example, there is very little change in both the time-mean level and the overall signal shape between the cycles plotted in Figure 2.2. An expert user would undoubtedly come to the same conclusion from a visual inspection of the pressure trace plotted in Figure 2.2(a). However, one can see in Table 2.2 that the amplitude of the first harmonic of vane passing is still changing significantly over the two periods plotted in Figure 2.2(a). Since simulations of this type are often performed to assess vibratory stresses during the design cycle of an engine, there is a clear advantage to the application of a more robust method of convergence assessment like that described here. For example, an 11% variation in the amplitude of unsteady forcing could well mean the difference between passing and failing an FAA certification test for resonant stresses.

To complete this example, Figure 2.3 is a plot of the fuzzy convergence level versus the periodic cycle number for 34 periodic intervals (i.e. 34 vane-passing events). The fuzzy sets that dictate the outcome of the overall level are also indicated on the figure. One can see that the convergence behavior of the simulation is in this case controlled by the variations of the magnitude and phase of harmonics of the fundamental vane-passing frequency from cycle-to-cycle. While this convergence behavior is typical of simulations where simple vane-blade interaction effects dominate the flowfield, the importance of tracking more than the Fourier

components as the solution progresses is illustrated below with reference to another turbine geometry.
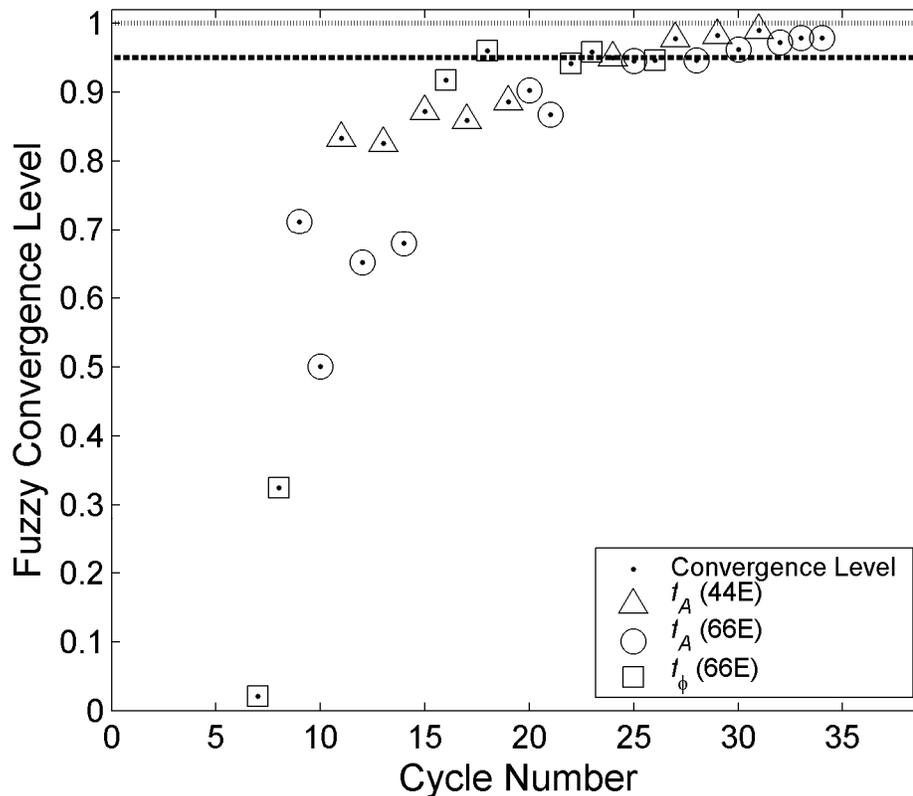
Figure 2.3: Convergence behavior of the flowfield at a location of interest on the blade pressure side for HPT1.

Again, it is important to recognize that the flowfield parameter selected for convergence monitoring is case dependent: the most important quantities are dictated by the reasons for performing the simulation. If the designer is assessing the expected level of resonant stress due to a specific forcing function on the airfoil surface, then the amplitude and phase angle at that frequency must be monitored at a number of locations on the airfoil surface. Alternatively, the amplitude and phase angle of the integrated aerodynamic load on the surface can be monitored. In addition, if the purpose of the analysis is to quantify a change in the time-mean performance resulting from the latest design iteration, then the mass- or mixed-out-averaged efficiency of the stage is the quantity to monitor.

One must also keep in mind that some quantities within the simulation converge well before others: for example, the pressure field typically becomes truly periodic well in advance of the entropy field due to the disparate propagation rates of finite pressure waves and viscous disturbances. So, great flexibility was built into the current implementation of the convergence-assessment algorithm described above. The user can monitor a large number of

flow quantities at any point in the flowfield. This is very useful when determining overall simulation convergence in post-processing mode. Also, one can estimate the convergence of arbitrary signals generated as the solution progresses (e.g. mass-flow rates, efficiencies, integrated airfoil loadings, etc.), and one can use that to control an unsteady optimization routine. Another example of the application of this algorithm to a periodic-unsteady flowfield predicted in the course of a resonant-stress analysis of a turbine is described below.

2.4   An Example of Atypical Convergence Behavior

Again, a primary reason for executing an unsteady CFD simulation during the turbomachinery design cycle is to predict airfoil resonant stresses. If vibratory stress problems are detected early enough during detailed design, then they can be mitigated, as we shall see later. However, if unacceptable vibratory stresses are discovered after the engine has been put into service, then life-cycle costs can increase significantly. Avoidance of these so-called "design escapes" is thus critically dependent upon accurate predictions of unsteady loads on airfoil surfaces.

Predictive tools for vibratory stresses typically rely on accurate Fourier analysis of time-resolved pressure fields [13, 14], and true periodicity is required to avoid errors resulting from spectral leakage and/or picket fencing effects [55]. Thus it is necessary for designers to quantify convergence levels prior to determining vibratory stresses, especially when such calculations require the transfer of data between analysis groups (e.g. aerodynamics and structures to aeromechanics). Airfoil surface static pressure fluctuations are the root cause of vibratory stresses, and when integrated over the airfoil surface, these static pressures provide the airfoil loading. So, time-resolved traces of the integrated airfoil loading can provide a suitable means to monitor convergence in such situations.

For another example of the performance of the present method, consider a stage-and-one-half calculation for a high-pressure turbine (HPT2) having airfoil counts equal to 36, 72, and 48 in the first vane, first blade, and second vane row, respectively. Here, $1/12^{th}$ of the wheel was modeled in the simulation with the purpose of the analysis to assess drivers due to the fundamental vane-passing frequencies only. The solution was run for 6 complete cycles from convergence of the steady-state flowfield, and inspection of Figure 2.4 reveals that convergence was not achieved on that interval in the current example. In fact, a convergence level of less than 0.7 was achieved for the axial force component.

Since the level of convergence achieved by the axial component was lower than that of all the others, it was selected for further investigation. Figure 2.5 is a plot of the normalized axial force signal as well as the membership grades in the fuzzy sets defined in Equations 2.6-2.10 as a function of periodic cycle number. The convergence level is dictated by the lowest membership grade over all the membership functions, namely, the fractional signal power, f_P.

A low level of f_P implies that there is significant unsteadiness due to an unexpected frequency. Also note that low levels of the cross-correlation at zero lag, f_S were obtained. This implies a significant change in signal shape from cycle-to-cycle, and this can mean that the primary periodicity occurs in the simulation over some unanticipated time-scale, calling into question the validity of the DFT results used throughout the method. In any case, the results suggest that rigorous interrogation of the unsteady flowfield predicted in the turbine is warranted.
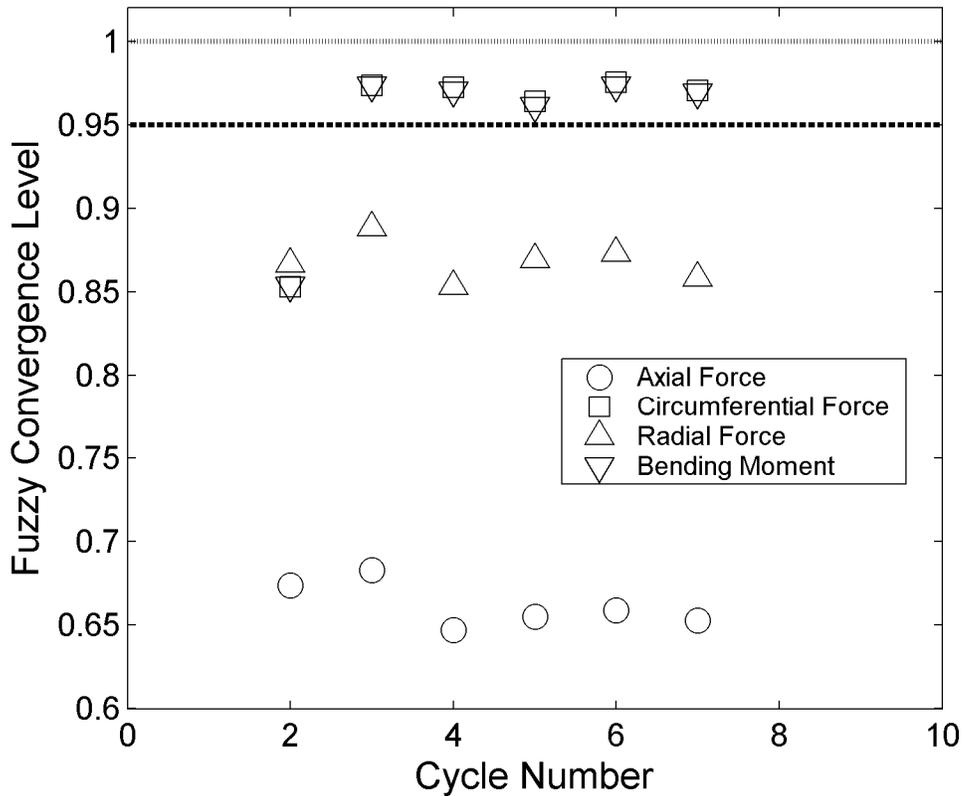
Fig. 2.4   Convergence levels for blade force components as a function of periodic cycle for HPT2

Figure 2.6 is a plot of fractional signal power due to engine orders of excitation up to 300. There is significant unsteadiness in the axial force exerted on the blade due to the first harmonic of the second-vane passing frequency, and this contributes to the low level of f_P. Consideration of the blade Campbell diagram might lead one to conclude that no resonance is to be expected due to that forcing function. However, more problematic is the signal power detected at the engine orders above 150. While 180E is the fourth harmonic of the first-vane passing frequency, the significant peak that occurs at 168E is spurious, and it warrants further investigation.
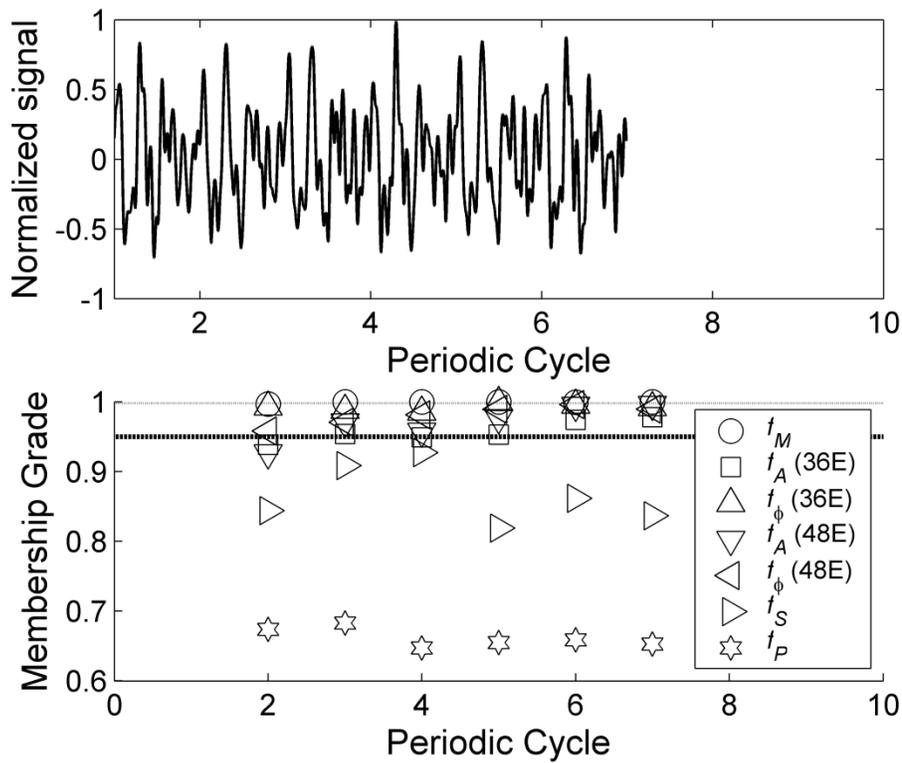
Fig. 2.5   Plots of time-resolved blade axial force and fuzzy-set membership grades as functions of periodic cycle (HPT2).
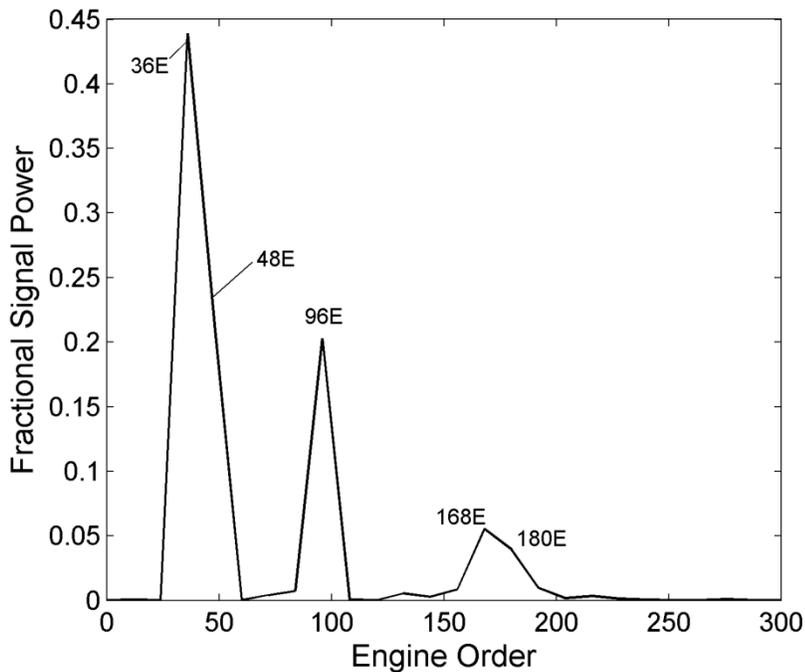
Fig 2.6   The results of a PSD analysis performed on cycle seven of the axial force signal for the blade of HPT2. Power contributions from unexpected frequencies are apparent.

Plots of normalized, time-resolved flow rates entering and exiting the blade row are plotted in Figures 2.7(a) and 2.7(b), respectively, along with fractional signal power as functions of frequency resulting from PSD analysis. One can see only the unsteady blockage effect of the upstream vanes in the inlet flow plots of Figure 2.7(a). In Figure 2.7(b), however, there is significant unsteadiness associated with the blockage of the downstream airfoils as well as high-frequency unsteadiness at 168E and 180E. A high-frequency blockage effect is suggestive of inherent unsteadiness (i.e. vortex shedding). Further, the unsteadiness is broad-banded and suggests that the shedding is actually occurring at a frequency between 168E and 180E with an attendant picket-fencing effect on the spectral analysis.
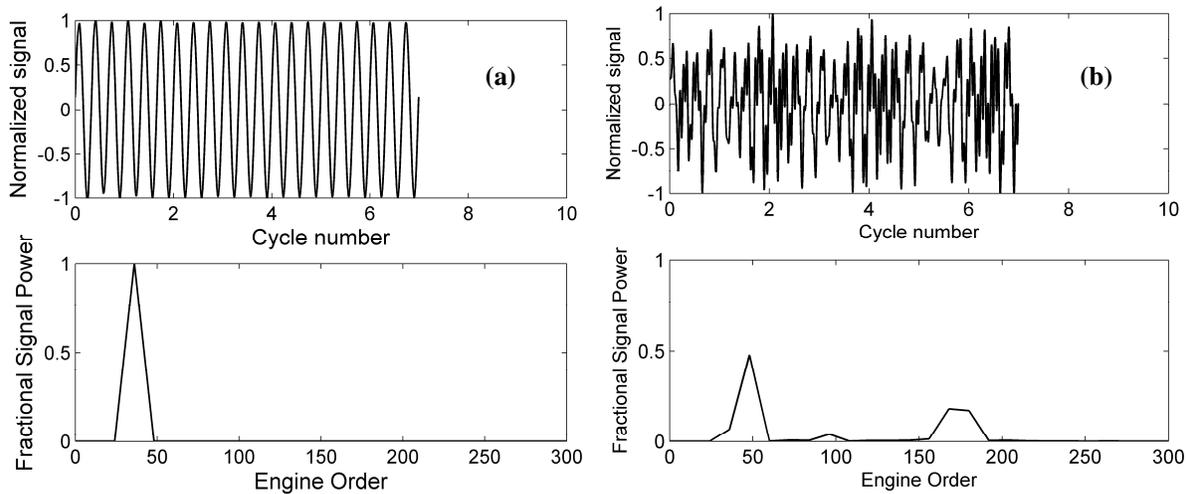

Fig. 2.7 **Normalized flow rate (a) into and (b) out of the blade row versus periodic cycle number and the results of a PSD analysis of the signal (HPT2).**

One can see additional evidence of vortex shedding in Figures 2.8 and 2.9. Figure 2.8 is a plot of the DFT magnitude calculated from the time-resolved entropy rise through the blade row at 168E ($\approx$ 31 kHz). A midspan plane is shown for a single blade passage, and the highest magnitude of the unsteady entropy rise is found in the vicinity of the blade trailing edge. Again, this is characteristic of vortex shedding. A calculation of the Strouhal number of the oscillations based on trailing-edge diameter and the local velocity in the vicinity of the trailing edge gives a value of $\approx$ 0.16. Figure 2.9 is a plot of the local DFT magnitude of unsteady static pressure at the same midspan plane for the 168E frequency. Very high level magnitude fluctuations in static pressure occur near the blade throat and downstream of the trailing edge at a location consistent with a reflected cross-passage shock. This leads to the very interesting conclusion that the unsteady blockage caused by the vortex shedding produces enough of an instantaneous variation in the throat area to cause a shock to form transiently with a frequency consistent with the von Karman vortices. Consequently exceptionally high levels of unsteady pressure occur on the blade suction side at the vortex-shedding frequency, and these affect the integrated load on the airfoil surface substantially.

These unsteady pressure variations would result in severe non-synchronous vibration in an operating engine, and while this is not normally encountered in turbines, it is a subject often discussed in the literature with respect to compressors [67, 68].
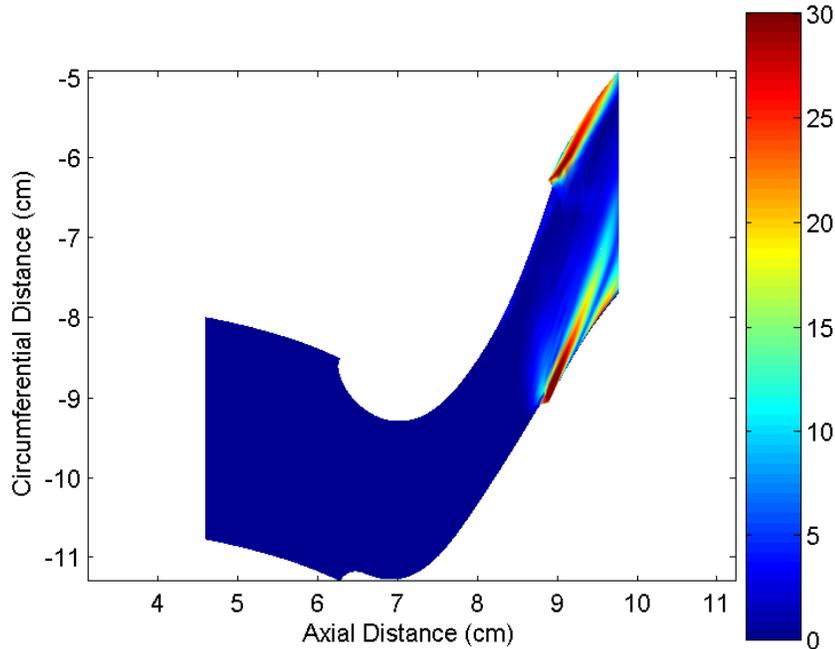
Fig. 2.8 **Contours of DFT magnitude at 168E calculated from time-resolved entropy rise (J/kg/K) at midspan through the blade passage (HPT2).**
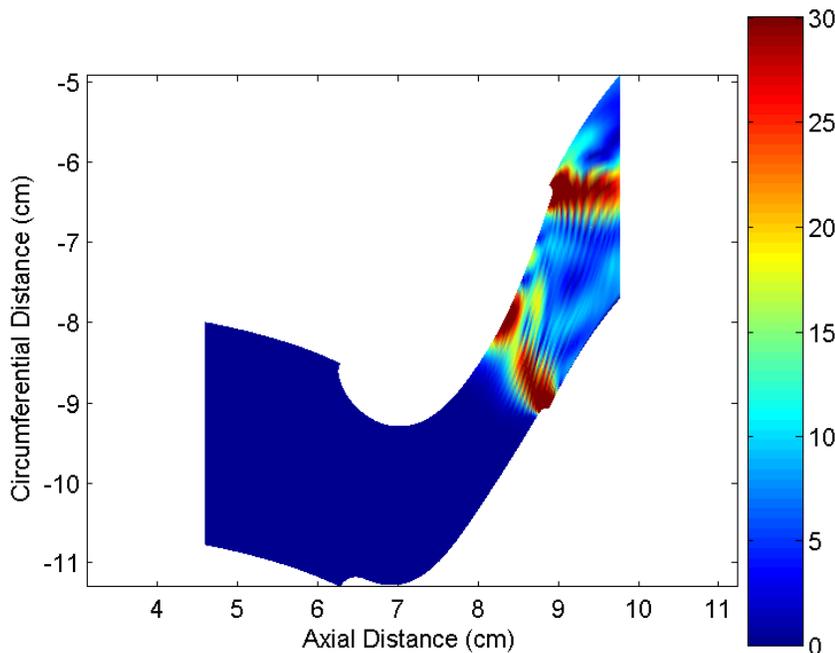
Fig. 2.9 **Contours of DFT magnitude at 168E calculated from time-resolved static pressure (kPa) at midspan through the blade passage (HPT2).**

Note that the simulation described above represents an early iteration in the design cycle for a turbine. In part as a consequence of these results, the design parameters of the turbine changed markedly before the final geometry was obtained. Consequently, no significant high-frequency unsteadiness occurred in the product. So, it is unclear whether or not the phenomenon described here could in fact lead to an airfoil failure. However, Doorly and Oldfield [69] have noted the presence of instantaneous local separation on a turbine blade in conjunction with shock passing, and their Schlieren images were suggestive of the occurrence of the phenomenon described here in the vicinity of the blade trailing edge. In any case, it is clear from this example that application of the present method to assess convergence in predictions of vane-blade interaction provides designers and analysts with significant direction as to the interrogation of the flowfield and the health of the design.

2.4   Conclusions

A quantitative method to assess the level of convergence of a periodic-unsteady simulation was described. The method was based on well known signal-processing techniques, and these were used in conjunction with fuzzy set theory to define a single overall convergence level of the simulation. The development of the method was illustrated with reference to predictions of vane-blade interaction in a pair of transonic high pressure turbines. It was shown that the technique is very useful as an indicator of the overall quality of simulations used to calculate resonant stresses as well as guide to further investigations of the flowfield and characterization of the design. In particular, the method was shown to be useful in detecting inherent unsteadiness in the flowfield of a high-pressure turbine, and therefore judicious application of the technique can be a significant factor in preventing design escapes.

3. Unsteady Interactions in the HIT Research Turbine

Armed with a means to assess the quality of a periodic-unsteady simulation of a turbine flowfield, it is now possible to discriminate among designs to achieve low levels of unsteady forcing. The turbine of interest in further comparative studies is the final design of the HIT RT. The HIT RT is a stage-and-one-half high pressure turbine that is consistent with a dual-spool engine that has an Overall Pressure Ratio (OPR) of 40 and is governed by basic cycle parameters that are shown emboldened in Table 3.1 for the constraint of a fixed flowpath. To design the test article, the flowpath of an existing experimental turbine was selected to keep costs of instrumentation (i.e. inlet and exit rakes) and static hardware manufacture to a minimum. Accordingly, the turbine design space was explored considering the following parameters: wheel speed, airfoil Zweifel coefficients, and stage reaction. Values for tip clearance, trailing-edge diameters, and blade taper ratio were set to constant levels that were consistent with state-of-the-art turbines.

Table 3.1. Cycle data (**emboldened**) and meanline design parameters (plain text) for the HIT RT.

	1V	1B	2V	2B
T3 (K)	**222**			
T4 (K)	**444**			
Inlet Flow Parameter [(kg/s) K $^{1/2}$ / kPa]	**1.13**			
Work Coefficient [(g J ?h) / U $_{mean}^2$]	----	2.08	----	2.01
Flow Coefficieny (C$_{x,exit}$ / U$_{mean}$)	----	0.71	----	1.2
Efficiency (%)	----	87.3	----	91.7
Pressure Ratio (Total-Total)	**----**	**3.75**	**----**	**1.85**
Reaction (%)	----	49.5	----	55.0
N / Tt,in $^{1/2}$ (RPM / K $^{1/2}$)	----	361	----	279
AN^2 x10^{-6} (m RPM) ^{2} [Engine / Rig]	----	37 / 8.4	----	21 / 4.8
Exit Mach Number	0.88	1.30 (rel)	0.89	0.94 (rel)
Turning (degrees)	77	115	11	80
Percent Cooling	**7**	**4**	**5**	**2**
Airfoil Count	23	46	23	69
Zweifel Coefficient	0.85	1.13	0.4	1.25

The HIT RT is consistent with many transonic High Pressure Turbines (HPTs) that are used in combination with contra-rotating Low Pressure Turbines (LPTs) in that the geometry of the inlet guide vane of the low turbine induces a reflection of the incident shock wave from the high turbine blade that propagates back upstream to impact the blade row that generated it. The net result of this unsteady interaction can be large levels of resonant stress and even a High Cycle Fatigue (HCF) failure. To illustrate the topology of the unsteady interaction that occurs in a contra-rotating multi-spool turbomachine, an instantaneous distribution of both static pressure and entropy from a 3D unsteady RANS calculation of the HIT RT is shown below in Fig. 3.1. Note that the HPT blade row rotates while the LPT vane row is stationary. The HPT blade is transonic with a design isentropic exit Mach number of 1.3. The flow through the blade row passes through a cross-channel shock wave that interacts with the suction-side boundary layer and reflects. This shock wave oscillates in position (See item (1) in Fig. 3.1). Additionally, an oblique shock emanates from the trailing-edge of the suction side of the blade and proceeds downstream. As it does so, it interacts with the shear layer from the adjacent blade row (2) and ultimately impacts the boundary-layer on the pressure side of the downstream vane. Since the blade is rotating, the position of this shock/boundary-layer interaction sweeps upstream with time (3). The shock reflects from the vane pressure side and this reflection also moves upstream as the blade rotates (4), ultimately becoming a pressure perturbation that also propagates upstream to influence the time-resolved pressure

and heat transfer on the blade suction side. Along the way, the reflected shock crosses additional shear layers and shocks that emanate from the upstream blades (5). Altogether the unsteady interaction is exceptionally complex, so it is prudent to base any attempt to mitigate the forcing function experienced by the HPT blade due to interaction with the downstream row on the basic physics of unsteady shock motion.
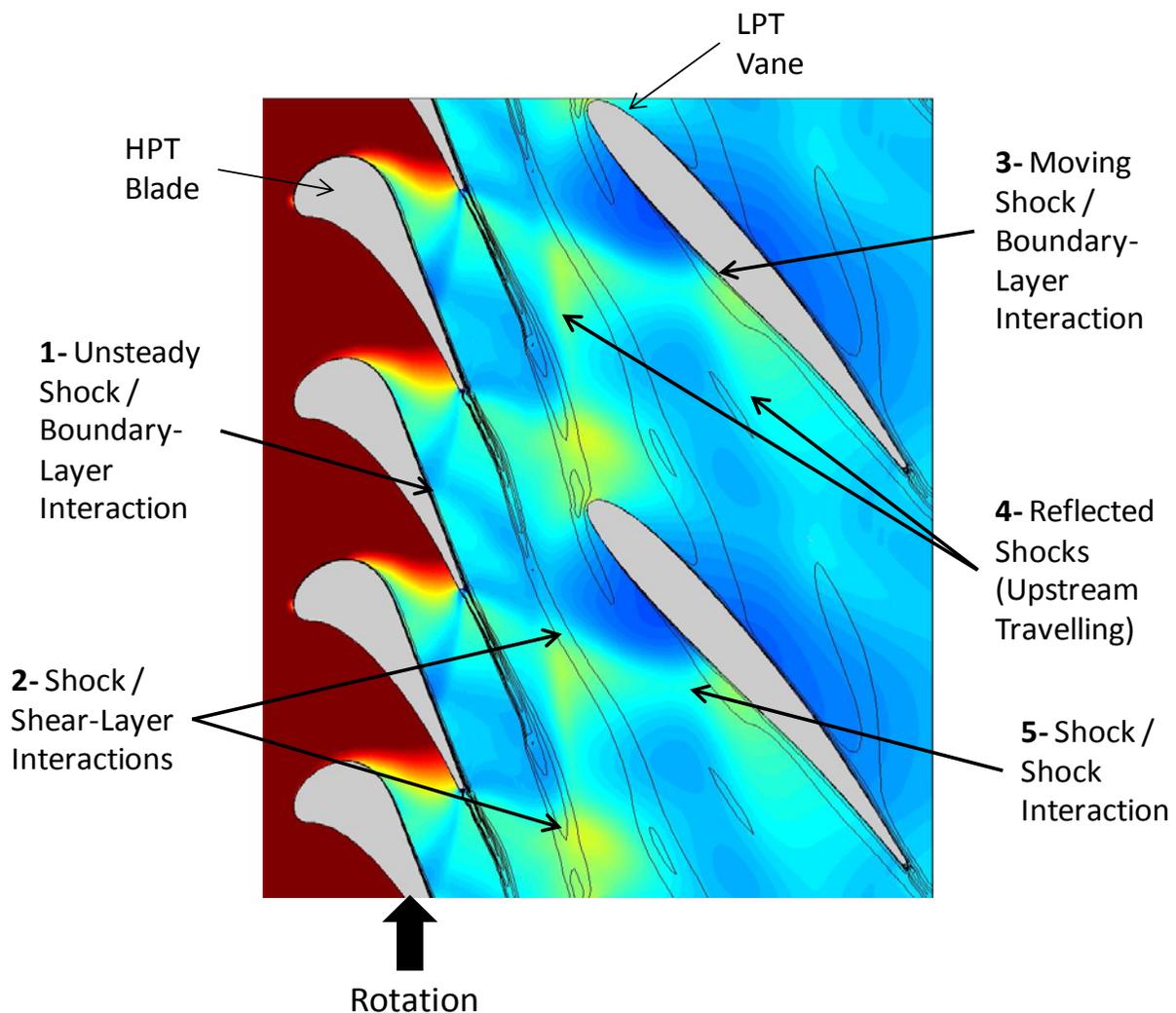
Fig. 3.1. The topology of unsteady interaction in a transonic turbine with a stationary downstream airfoil that is consistent with contra-rotation.

Other characteristics of periodic unsteady flows that are commonly observed in turbines like the HIT RT are illustrated in Fig. 3.2, below. The reaction of the turbine is near 50%, and consequently, the exit Mach numbers of the upstream vane and blade rows are 0.88 and 1.30, respectively. So, the flow capacity of the turbine is set by the blade row, and the cross-passage shock that travels from the pressure side of one blade to the suction side of the adjacent blade (See location 1 in Fig. 3.1, above), represents the choke plane of the stage.

Accordingly, any unsteadiness observed upstream of the intersection of the pressure-side shock with the blade suction side is attributable to the stage inlet vane, while any that occurs downstream comes from the LPT guide vane. This location is clearly evident in Fig. 3.2 which is a pair of plots that represent the unsteady pressure on the blade suction side in terms of the percent signal power (See Section 2.2 above) due to the fundamental- and the first harmonic of the downstream vane-passing frequency. These frequencies are given non-dimensionally as "engine orders" that represent the frequency of excitation normalized by the frequency of revolution of the blade row in Hz. The engine order associated with the fundamental passing frequency of an airfoil is consistent with the number of airfoils in that row. Here one can see that the interaction of the blade with the upstream airfoil row is dominated by the fundamental vane-passing frequency (1 x 2VPF=1 x 1VPF), whereas the signal power associated with the downstream vane row occurs primarily at the first harmonic of airfoil passing (2 x 2VPF). This behavior is very often seen in turbine engines with single stage HPTs and contra-rotating downstream LPTs that have inlet guide vanes.
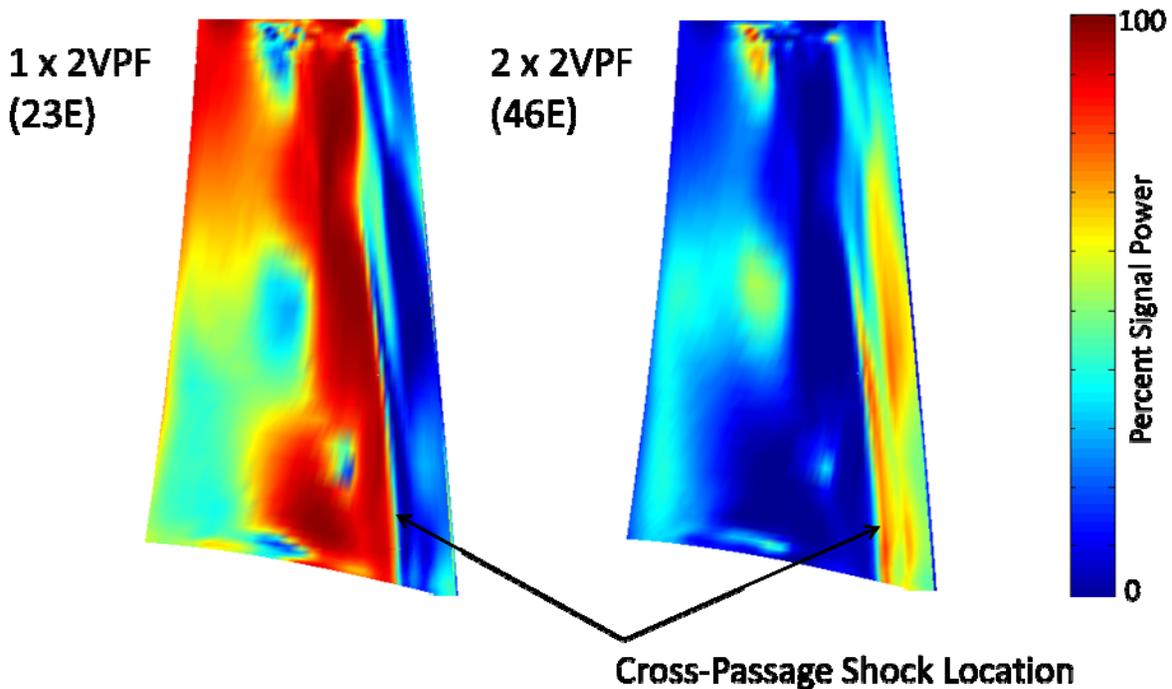

Fig. 3.2. Blade unsteadiness due to downstream interaction is often dominated by the first harmonic of the vane-passing frequency in single stage HPTs with vaned contra-rotating LPTs.

3.1   Validation of Predictions of Transonic Blade Loadings in the HIT RT

The importance of validating design-level predictions of time-resolved airfoil loads cannot be over-stated. A demonstrated capability to predict unsteady pressures on airfoils accurately gives the designer confidence in his ability to detect and/or to deter resonant-stress problems in development engines. To have greatest efficacy in reducing life-cycle costs, such code validation is ideally undertaken proactively: verification studies are performed in relevant environments on an ongoing basis whether or not there is a resonant-stress problem in need of solution. The payoff for such a process was illustrated in [70] where design optimization techniques were used successfully to predict and to control the level of unsteady forcing in a gas turbine engine during the design cycle. In that study, the maximum level of unsteady forcing that occurred on the blade surface due to potential-field interaction with the upstream vane row scaled directly with the peak-to-peak amplitude of the predicted steady-state static pressure variation in the circumferential direction at the vane exit.   This knowledge, combined with prior benchmarking of predicted levels of unsteady forcing functions in a similar high-pressure turbine stage [71] enabled analysts to reduce resonant stress levels for a transonic turbine blade during the design cycle.

As of this writing, installation of the HIT RT in the AFRL Turbine Research Facility is complete and rotor-dynamic checkouts are underway. Initial testing of the HIT RT is meant to validate design-level analysis methods for the prediction of vane-blade interactions. The complex shock interactions in the stage-and-one-half HIT Research Turbine are driven by the transonic flowfield over the rotating airfoil. So, in the mean time, it is prudent to study the aerodynamics of the blade row in isolation and determine the ability of design-level simulations to assess the flow physics in a nominally steady flow prior to testing in a rotating turbine stage. The Transonic Cascade Facility at AFRL was developed over the last several years in order to make such assessments. The facility allows for independent variation of both Reynolds number and airfoil exit Mach number, so it is well suited for this purpose. Fig. 3.3 is a set of measured and predicted normalized static pressure variations around the surface of the midspan section of the HIT RT blade row in cascade. The analyses were conducted prior to the experiments, so they are true predictions. The design exit Mach number for the airfoil is 1.3. One can see that the transonic flowfield around the airfoil is quite well predicted over a range of Mach numbers from subsonic through the transonic regime until limit loading of the airfoil is achieved (Mach 1.75). At limit loading the shock that occurs across the passage runs from the pressure-side trailing edge of one airfoil to the suction-side trailing edge of the adjacent airfoil. This is the strongest shock that can possibly occur in the airfoil row, and it represents a total-to-total pressure ratio in excess of 5 for a turbine with a design pressure ratio level of 3.75.
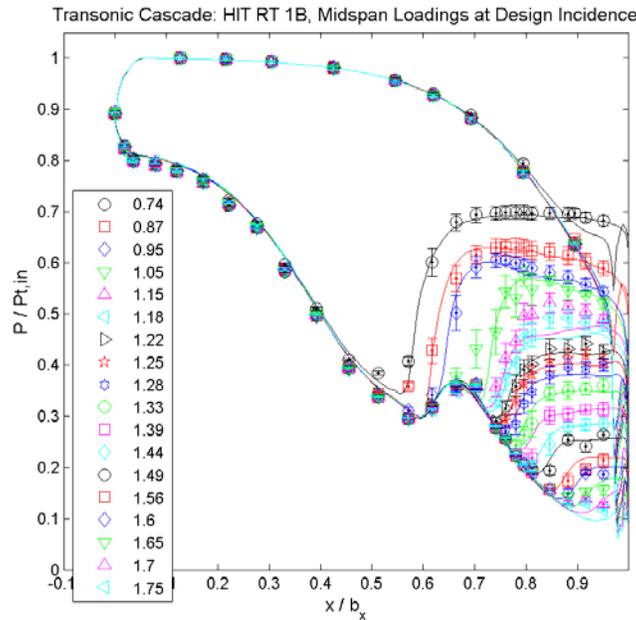
Fig. 3.3. Normalized static pressure loadings over the HIT RT blade row in a transonic cascade facility. Both data and predictions are shown for various isentropic exit Mach numbers listed in the legend.

3.2   Computational Methods

The turbine cascade above was analyzed with the Reynolds-Averaged Navier Stokes (RANS) solver of Dorney and Davis [63], and that code was also used exclusively in the aerodynamic design phase for the initial build of the HIT RT. However, all design studies presented below were undertaken with the 3D, multi-stage RANS code described by Ni et al. [72].   The code employs implicit dual time-stepping to solve for the periodic-unsteady flowfield on an OHHH-grid topology, and numerical closure is obtained via the k-ω turbulence model of Wilcox [73]. The code is accurate to second-order in both space and time. The flow solver employs a finite-volume, cell-vertex Lax-Wendroff [74] method, and both local time-stepping and multi-grid techniques are used to obtain rapid convergence.   For time-accurate calculations of rotor/stator-interaction with the Ni code, the flowfield is solved on a portion of the annulus over which spatial periodicity occurs. This is not arduous for the HIT RT as periodicity occurs on $1/23^{rd}$ of the annulus (See Table 1, above). However, some airfoil scaling (< 5% of pitch) is used to make the asymmetric analysis described in section 4.5 below more tractable. One cannot expect a simulation with airfoil scaling to give a quantitatively accurate prediction of unsteady forcing (See, e.g. [71]). However, airfoil scaling should reveal the qualitative trend seen with asymmetric spacing, and that is acceptable for the illustrative purposes of the example given below.

4. Design for Reduced Shock Interaction

As seen above, when an HPT is used in combination with a contra-rotating LPT significant unsteadiness can arise at the first harmonic of the downstream vane passing frequency. Because of this the airfoil count of the downstream vane in state-of-the-art turbines is selected typically to move the resonant frequencies due to this interaction outside of the operating range of the HPT. While this is an acceptable solution to an engineering problem, it typically requires an increase in the airfoil count. Consequently, both engine weight and life cycle costs also increase. This is particularly wasteful because the turning requirements of the downstream vane are quite low as compared to other airfoils in the turbine, suggesting low part counts and weight if one considers the aerodynamics of the components only.

In this section the HIT RT is used as a platform to investigate methods of altering the forcing function on the turbine blade via fluid dynamic means. This amounts to a series of design studies aimed at either a reduction of the magnitude of the unsteady pressure at twice the downstream vane passing frequency or an alteration of the phase of the interaction. These studies are not presented as an exhaustive list: instead they are meant to illustrate what one might do in an effort to solve a resonant stress problem during the design cycle of a turbine. In all, six different methods are attempted, and it is possible to divide these into two main categories: design studies targeted at reducing the strength of the incident shock and those that affect shock reflections from the downstream vane. Under the first category, the results of two attempts to re-design the blade shape are presented. The first attempt focuses on a reduction of the steady peak-to-peak distortion in static pressure downstream of the blade while the second seeks to alter the distribution of loading on the blade surface. Under the second category, four different techniques are tried. These include altering the 3D shape of the vane to focus the shock reflections onto a different part of the blade suction side as well as a novel flow-control method to reduce the unsteadiness globally that involves steady blowing from the pressure side of the downstream airfoil row [75]. Additionally, the effects of downstream vane asymmetry and vane-to-vane clocking are investigated. The former technique acts primarily on the magnitude of the vane-blade interaction while the latter is more effective at altering the phase distribution of the unsteadiness. Again, the investigations of these concepts are at present strictly analytical. However, many of them are targeted for inclusion in future builds of the HIT RT and hardware is in various stages of manufacture and/or instrumentation installation. Also, while the techniques described are simply proofs-of-concepts, many of them are suitable for implementation in a design optimization system. Further, the actual adoption of these techniques for insertion in an engine would be very much dependent on the resonant mode targeted and the stage of the development cycle where a vibratory stress problem is detected and/or diagnosed.

4.1   Blade Re-Design for Reduced Circumferential Distortion in Exit Static Pressure

The blade row of the initial build of the HIT RT was designed for minimum loss, and this was accomplished via both traditional (i.e. designer directed) methods and design optimization techniques. Many thousands of blade profiles were analyzed, and the complete design loop through 3D unsteady RANS was closed 22 times to give the final geometry of the experimental turbine. This resulted in what is often called a "balanced shock" blade design. The flow over the blade suction side experiences a pair of compressions of approximately equal strength. Here, further design iterations were conducted to reduce the pitchwise variation in static pressure downstream of the blade without concern for the effect on blade loss. Clark et al. [70] showed that reducing the circumferential distortion in static pressure exiting the inlet guide vane row can have a substantial effect on the severity of both unsteady pressures and resonant stress due to vane-blade interaction. In that work, the vane exit Mach number was approaching unity but still subsonic, so the unsteadiness was primarily due to potential field effects. However, Joly et al. [76, 77] have recently shown that the same attention to vane distortion is also beneficial for lower reaction machines that have supersonic vane exit Mach numbers. So, it is reasonable to surmise that attention the level of circumferential distortion in static pressure at the blade exit might yield a benefit in this case as well.

In Fig. 4.1 one can see both the midspan profile of the HIT RT blade (here denoted as the Baseline blade) and that of the airfoil designed for decreased exit static pressure distortion (designated the Low dP 1B) along with the loadings for each profile. In comparison with the HIT RT profile, the Low dP 1B has reduced trailing-edge diameter and wedge angle along with lower uncovered turning. The lower level of uncovered turning is consistent with the results of [70] where the same occurred in the re-designed vane. The balanced shock feature of the HIT RT is evident in the loading, and the pressure distribution on the re-designed airfoil is perhaps more indicative of this phenomenon. For the re-designed profile the steady level of the peak-to-peak variation in static pressure in the circumferential (pitchwise) direction was reduced 25% relative to that of the HIT RT blade. The results of 3D unsteady RANS analyses for the HIT RT with both the original and re-designed blades are shown in Fig. 4.2 as color maps of unsteady pressure magnitudes on the blade suction sides at twice vane-passing frequency. One can see a clear reduction in unsteadiness on the suction side of the blade downstream of the cross-passage shock. This would have a global effect on resonant stresses that might arise from the unsteadiness in this location. So, it is beneficial to the blade to reduce the strength of the shock that emanates from the blade suction-side trailing edge. This is a straightforward extension of the work presented in [70, 76, and 77]. Again, it was shown in [70] that such a reduction in unsteady pressure can yield a corresponding decrease in resonant stresses occurring on an airfoil in an operating demonstrator engine.
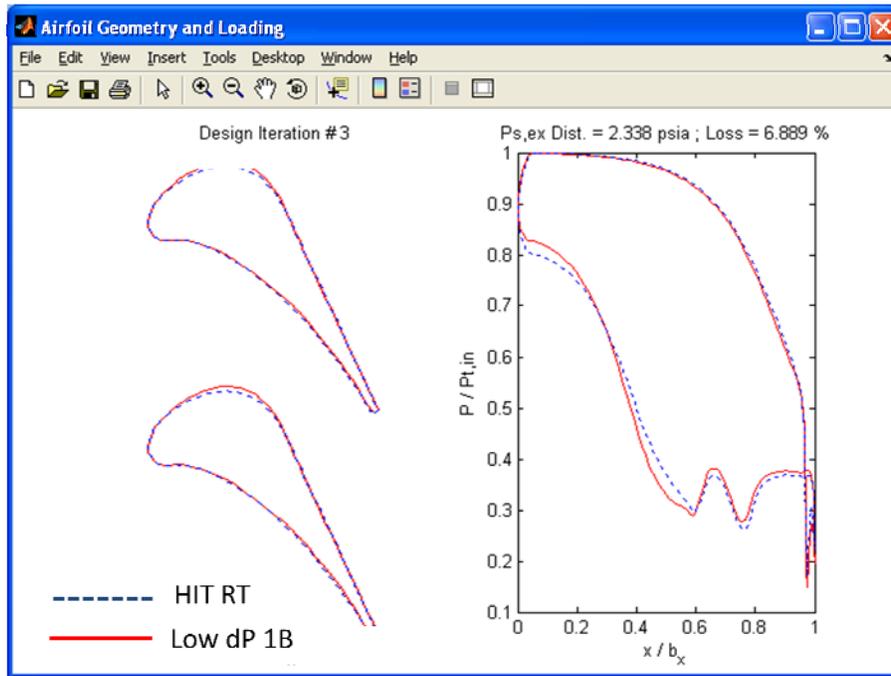
Fig. 4.1. Blade profiles and loadings for both the HIT RT at midspan and the airfoil designed for reduced static pressure variation at the exit of the row.
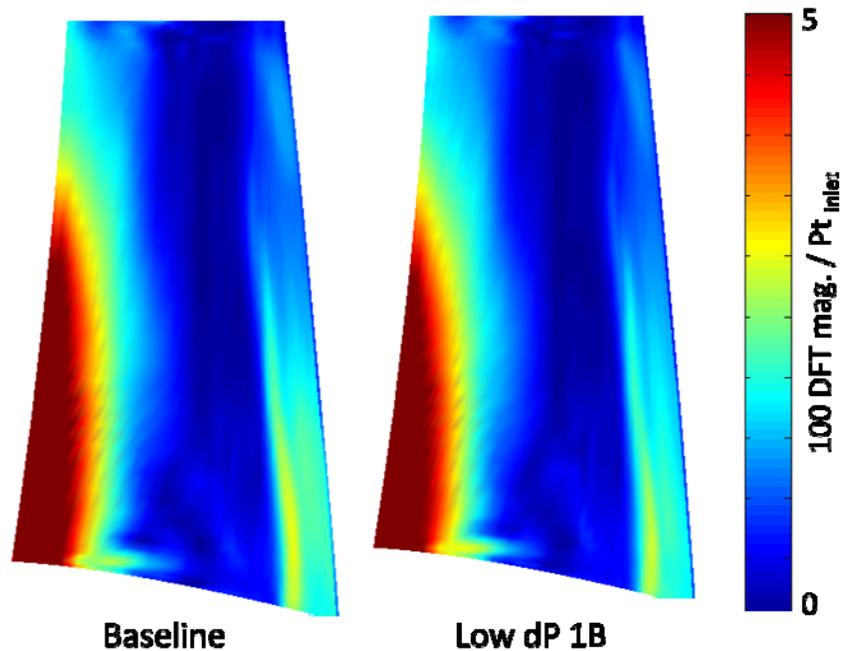

Fig. 4.2. Magnitudes of blade suction side unsteadiness at twice downstream vane passing frequency for the HIT RT (Baseline) and the Low dP 1B.

4.2 Blade Re-Design to Aft-Load the Profile

At first blush it is tempting to say that the large unsteadiness that occurs at twice vane passing frequency is a result of either the simplified airfoil counts of the HIT RT (1V/1B/2V = 23/46/23 is periodic on 1/2/1 airfoils) or the balanced shock feature of the blade with its attendant pair of compressions on the suction side. In regard to the former, it was stated above that the first harmonic of the downstream airfoil passing frequency typically dominates the signal power experienced by the blade in the region affected by shock reflections in any high work HPT with a vaned contra-rotating LPT. Examples of this phenomenon for turbines with much different periodic intervals are readily found in the literature. To take just one example, the turbine in the experiment of [71] had counts of 36/56/36 which is periodic on 9/14/9 airfoils, and still the dominant unsteady frequency due to blade and downstream vane interaction was the first harmonic of passing and not the fundamental. In regard to the latter, a simple design study is illustrative.

The HIT RT 1B was re-designed to aft load the blade, and this resulted in an airfoil profile that was much closer to limit loading than the baseline airfoil (See Fig. 4.3). The most obvious design change from the baseline airfoil to the re-designed profile, which is designated the Single Shock 1B is a significant increase in the uncovered turning. The HIT RT blade has almost none, while the re-designed blade has 8 degrees of unguided turning. The flow over the suction-side of the aft-loaded profile which results due to the increased uncovered turning experiences a single compression instead of a pair of pressure rises. Still, if one considers Fig. 4.4 there is significant unsteadiness on the blade suction side downstream of the cross-passage shock at twice the vane-passing frequency. In fact, it is clear that the re-designed blade is subjected to *greater* unsteadiness in this region at the first harmonic of downstream passing than the baseline (i.e. HIT RT) blade. Upon further reflection, this is no surprise. One must remember that periodic unsteadiness in a turbine is likely not well described by a single sinusoidal variation. The presence of harmonics of the fundamental passing frequency is not necessarily linked to an identifiable physical phenomenon like the pair of compressions on the HIT RT blade suction side. Further, aft loading the blade causes the cross-passage shock to occur at a higher Mach number. It is therefore a stronger shock that causes an increase in the peak-to-peak pitchwise static pressure distortion exiting the blade row. This in turn raises the unsteadiness over that portion of the blade suction side that is exposed to shock reflections from the downstream vane row.
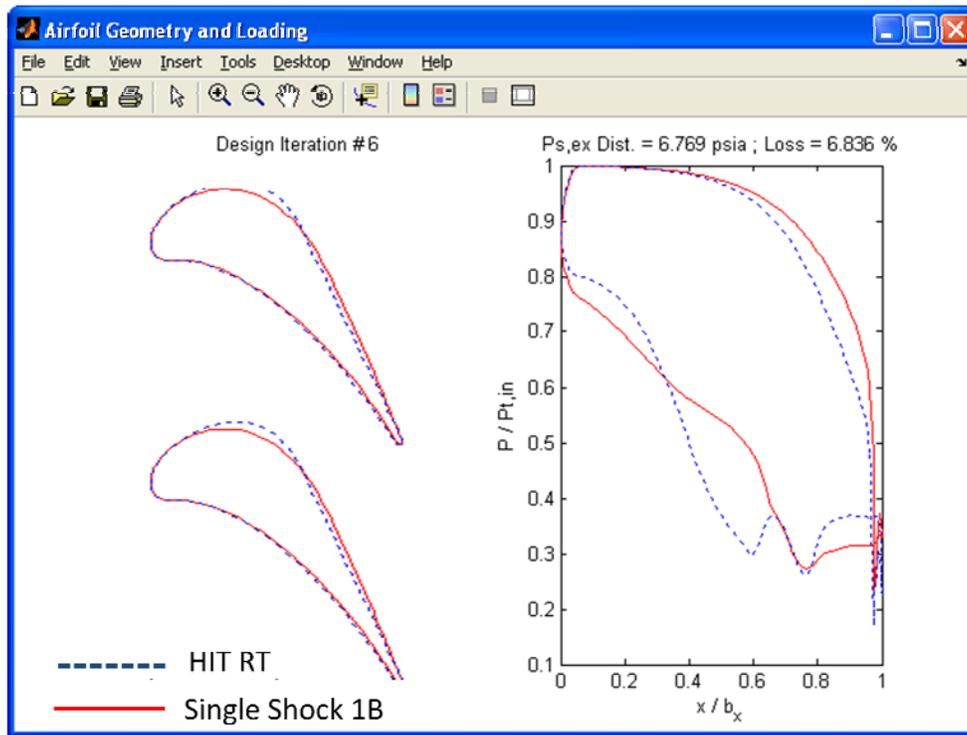
Fig. 4.3. Blade profiles and loadings for both the HIT RT at midspan and the airfoil re-designed for aft-loading.
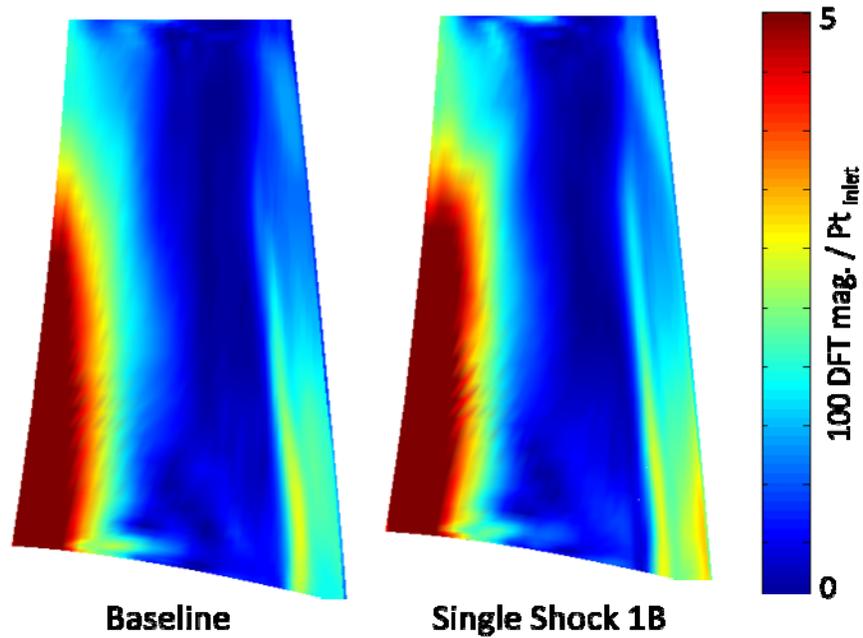

Fig. 4.4. Magnitudes of blade suction side unsteadiness at twice downstream vane passing frequency for the HIT RT (Baseline) and the Single Shock 1B.

4.3 Vane 3D Shaping

While the two previous sections concerned the effects of altering the transonic flowfield over the blade surface in an attempt to influence the interaction with the downstream vane, this one and the three following are concerned with altering the reflection of shocks from the vane in some way. At this point it is worth considering the basic physics of inviscid, unsteady shock motion to find a way forward. It is well known that a moving shock wave like that extending downstream from the rotating blade of the HIT RT induces a small velocity component normal to the shock and near coincident with its direction of travel. The moving shock wave must reflect from any stationary solid boundaries it impacts in order to maintain the no-slip condition at the surface. Further, the portion of the induced motion that must be cancelled is the vector component normal to the surface of the boundary. So, it stands to reason that if the local normal vector of the surface is altered, then the direction of travel of the reflected shock must also change. One can imagine a situation where the 3D geometry of the downstream vane is altered in such a way that the shock reflections from it are directed at a region of the upstream blade that is less likely to experience high resonant stresses.

In the initial design of the HIT RT downstream vane, the only three-dimensionality that was included was a consequence of the local variation in inlet and exit air angles that were specified as a result of design iterations at the meanline level. The vane was specified in 3D by stacking 2D profiles on the centroids of area of each section, and the geometry of the airfoil that resulted is shown in the center of Fig. 4.5. As an illustration of the effects of 3D shaping on vane-blade interaction, a pair of additional vanes was generated. For these airfoils the 2D profiles at each radius specifying the HIT RT vane was not altered. Instead, the location of the centroid of each 2D section of the airfoil was allowed to shift by an increasing amount of the pitch in either the positive or negative circumferential direction. The airfoils that resulted were called the bowed and reverse-bowed airfoils, and one can see these vanes on the left and right sides of Fig 4.5, respectively.
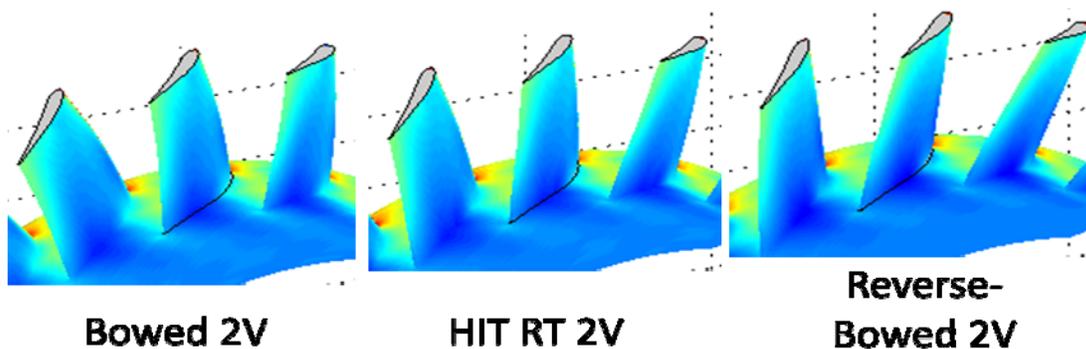

Fig. 4.5. Airfoils used to assess the effect of 3D shaping on vane-blade interaction.

The effect of 3D aerodynamic shaping of the downstream vane on the unsteady pressure experienced by the blade on the suction side is presented in Fig. 4.6 along with the baseline levels for the HIT RT. The effect of vane bow on the distribution of unsteadiness is profound. Reverse bowing tends to drive the unsteady pressure at the first harmonic of vane passing (2 x 2VPF = 46E) toward the blade tip while bowing focuses it near the hub. Independent of the mode shape, there is far less airfoil motion near the blade root than the tip. Consequently, driving the unsteady pressures toward the hub is a benefit when one considers resonant stresses. Also, 3D shaping of the vane alters the distribution of phase angles over the blade suction side downstream of the cross-channel shock. Fig. 4.7 is a plot of the variation in phase angle with span at approximately 95% axial chord due to the baseline vane as well as the bowed and reverse-bowed airfoils. One can see that the variation in phase angle with span is greater with 3D shaping than for the baseline vane. Resonance of course requires that unsteady pressures at a given frequency are coincident with a mode shape. It also requires that the phase of the unsteadiness is consistent with the oscillation of the airfoil. One expects, then, that a greater variation in phase angle over the region of the blade impacted by shock reflections is also beneficial from the standpoint of resonant stresses. However, one can truly assess the net benefit (or possibly detriment) of a variation in phase only through a complete vibratory-stress analysis.
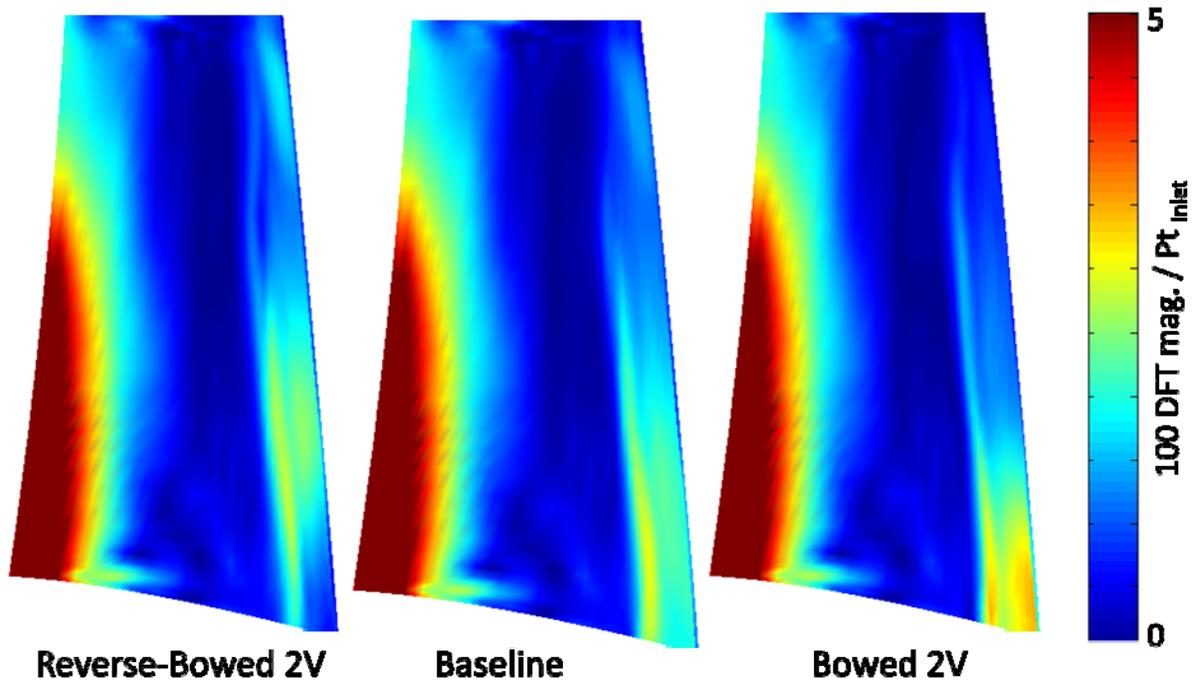

Fig. 4.6. Magnitudes of unsteadiness on blade suction sides at twice downstream vane passing frequency for the HIT RT (Baseline) and the Reverse-Bowed and Bowed 2V.

There are many examples in the literature of 3D shaping of airfoils, although often the goal of such designs is to achieve a benefit in aero-performance. One exception is the design optimization study of Joly et al. [76, 77] where the geometric parameterization of the upstream vane was consistent with both bow and lean of the airfoil. As noted above, Joly et al. sought to reduce the circumferential distortion in static pressure exiting the vane row in an effort to decrease t he unsteadiness on the blade. However, unlike in the current study where a modification of shock reflections is sought, the work of Joly et al. was more consistent with the example in section 4.1 where the goal was to reduce the strength of incident shocks in the HIT RT.
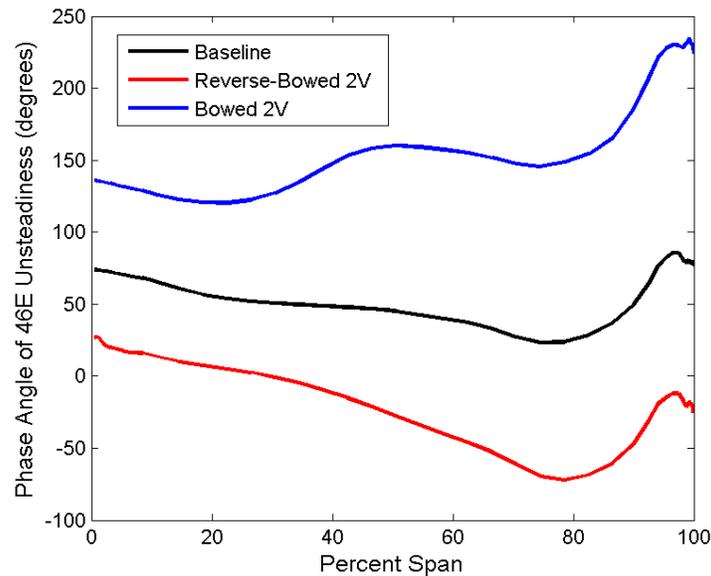

Fig. 4.7. The variation in phase angle of the unsteady pressure with span on the blade suction side at approximately 95% chord for the twice vane-passing frequency (46E).

4.4 Vane Pressure-Side Blowing

As stated in the last section, shock reflections from the downstream vane of the HIT RT arise physically because of fluid friction on the vane surface. From that it follows that having a net velocity component at the surface of the vane might reduce or even obviate shock reflections in the HIT turbine. Here we check the idea that inducing a velocity component from the surface in a manner similar to film cooling might reduce the unsteadiness that arises on the blade suction side due to shock reflection [75]. Paniagua and his co-workers [78, 79] have looked at pulsed trailing-edge flows on the blade for the purpose of what amounts to incident-shock control in the context of this lecture. For this study mass injection through a series of more than 1100 discrete holes on the pressure side of the *downstream* vane was simulated. The flow was specified simply as normal to the local surface of the vane, and a pair of levels of mass flow as a percent of the mainstream level was simulated. The results are plotted in Fig. 4.8 as levels of DFT magnitude at twice vane passing frequency on the blade suction

side. It is clear that aspiration from the vane pressure side does have a global effect on the overall unsteadiness downstream of the cross-passage shock on the blade suction side. At 1.7% flow there is a small but discernible effect whereas at 6.8% flow the reduction is quite dramatic. While there is no chance that an aerodynamic designer would allow the use of 6.8% mainstream flow for this purpose, 1.7% is consistent with the amount that one might expect to use for film cooling in a high work turbine. And while there is an aero-performance penalty for film cooling, it was found that reducing the unsteadiness on the blade suction side was also associated with a predicted decrease in time-mean losses on the blade. Clearly, this is a case where one might find that clever use of available film cooling flows could have a net benefit on the overall design of the system.
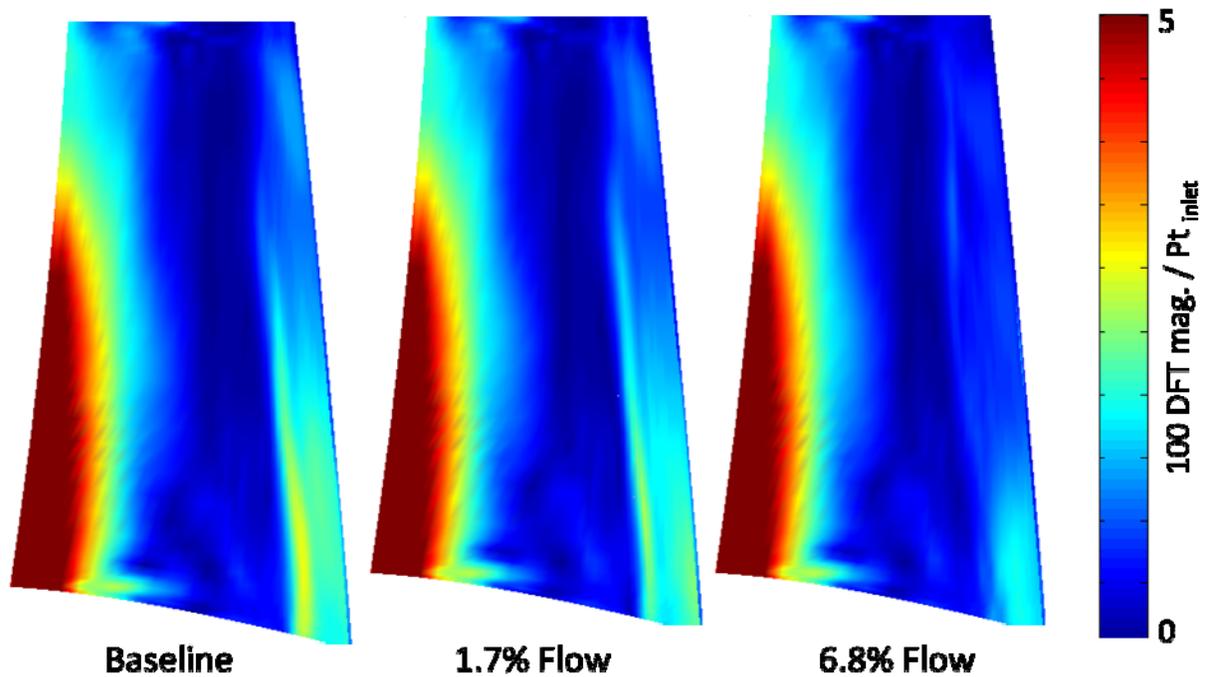

Fig. 4.8. The effect of aspiration from the downstream vane pressure-side on blade suction-side unsteadiness at twice the vane-passing frequency. It is clear that mass injection globally affects the unsteadiness on the blade aft of the cross-passage shock.

4.5 Vane Asymmetric Spacing

It is well known that asymmetric airfoil spacing can result in decreased levels of unsteady forcing at specific frequencies [70, 80-83]. The earliest study of non-uniform airfoil pitch by Kemp et al. [80] relied on simple Fourier methods to predict the effects of asymmetric vane spacing on resonant stresses. The authors then compared measured levels of stress with both uniform and non-uniform vane pitches, achieving agreement with their predictions. In more recent years modern CFD tools [81] and design methodologies [82, 83] have been used to assess the effects of vane asymmetry in both turbines [70] and compressors [81], and

successful reductions in forcing have been achieved in operating demonstrator engines [70]. Here we follow the analysis technique and methodology outlined in [70] to set up and determine the effect of downstream vane asymmetry on unsteadiness in the HIT RT. An asymmetric vane ring composed of two ½-wheels having vane downstream counts of 24 and 22 was analyzed by applying a modicum of airfoil scaling to the first vane and blade rows in each simulation. This gave model counts for analysis of 24:48:24 and 22:44:22, respectively, and each of these has a 1:2:1 airfoil-count ratio. Each simulation was run to periodic-unsteady convergence, and the solutions were then post-processed for one half revolution. The time histories of unsteady pressures on the blade surface were then concatenated in time to complete a full revolution while paying careful attention to the location of the blade in space at the time of intersection for the two signals.

Fig. 4.9 is a plot of DFT magnitudes versus engine order for the asymmetric vane-spacing case compared to the results of analyses with symmetric airfoil counts of 22, 23 (i.e. the HIT RT or Baseline count), and 24. The DFT of the periodic-unsteady pressure was calculated on the blade suction side at approximately 95% axial chord and 10% span. So, the location in question was well downstream of the location of the cross-passage shock, and it is therefore subject to unsteadiness arising from shock reflections off the downstream vane only.
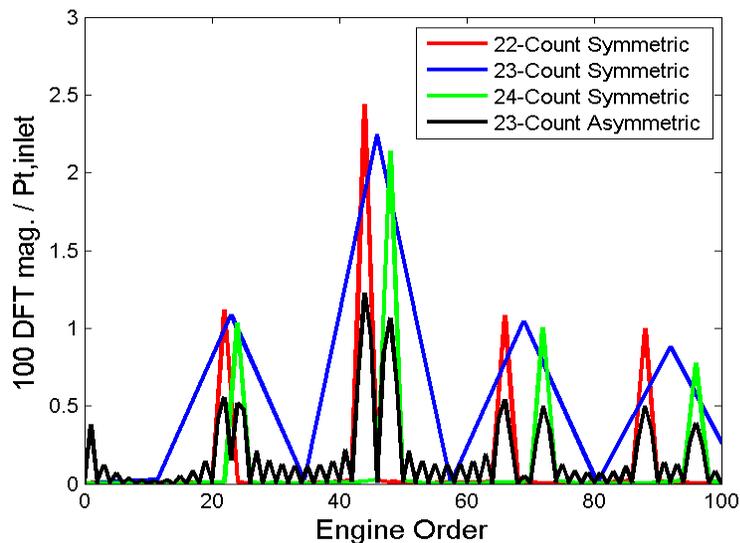

Fig. 4.9. Asymmetric vane-spacing results in a significant reduction of 1B unsteadiness levels at the fundamental vane-passing frequency and its harmonics at 95% chord, 10% span on the blade suction side.

Asymmetric vane spacing has four major effects on the DFT magnitude of the unsteady pressure as compared to a symmetric-count analysis. First, asymmetry reduces the DFT magnitude at the fundamental and first harmonic of vane passing by more than 50% relative to that occurring in the case of symmetric spacing. Second, asymmetry acts to spread the signal power that was distributed among a small number of frequencies consistent with the

fundamental and harmonics of vane passing to additional frequencies. That is, where initially there was signal power at 23E, there is now unsteadiness at both 22E and 24E. Additionally, there is some sharing of signal power among frequencies somewhat lower and somewhat higher than the 22E and 24E frequencies. Third, there is low engine-order excitation associated with creation of the new spatial periodicity of the asymmetric vane ring: the wheel is now spatially periodic on the full revolution of the blade. Fourth, there is now low power unsteadiness occurring at all multiples of the frequency resolution of the simulation [i.e. Δf =1/(NΔt)]. Taken collectively these results are an indication that asymmetric vane spacing is substantially beneficial for reducing the severity of resonant stresses due to crossing associated with vane passing. However, asymmetry can affect resonant stresses arising from low engine-order crossings negatively. All these results are quite in keeping with known effects of asymmetry that one can glean from the available literature [70, 80-83].

It is worth noting that asymmetry has an effect on unsteadiness over the entire region of the blade affected by shock reflections from downstream. That is, the effects seen in Fig. 4.9 are not a local phenomenon associated with the specific point selected for comparison in the figure. One can see this in Fig. 4.10 where the magnitude of the unsteadiness predicted on the blade suction side in the baseline HIT RT at twice downstream vane passing is compared to the 44E and 48E DFT magnitudes predicted for the asymmetric vane ring. Clearly, one can extend the comparison of symmetric and asymmetric analyses presented with reference to Fig. 4.9 to the rest of the blade suction side downstream of the cross-channel shock.
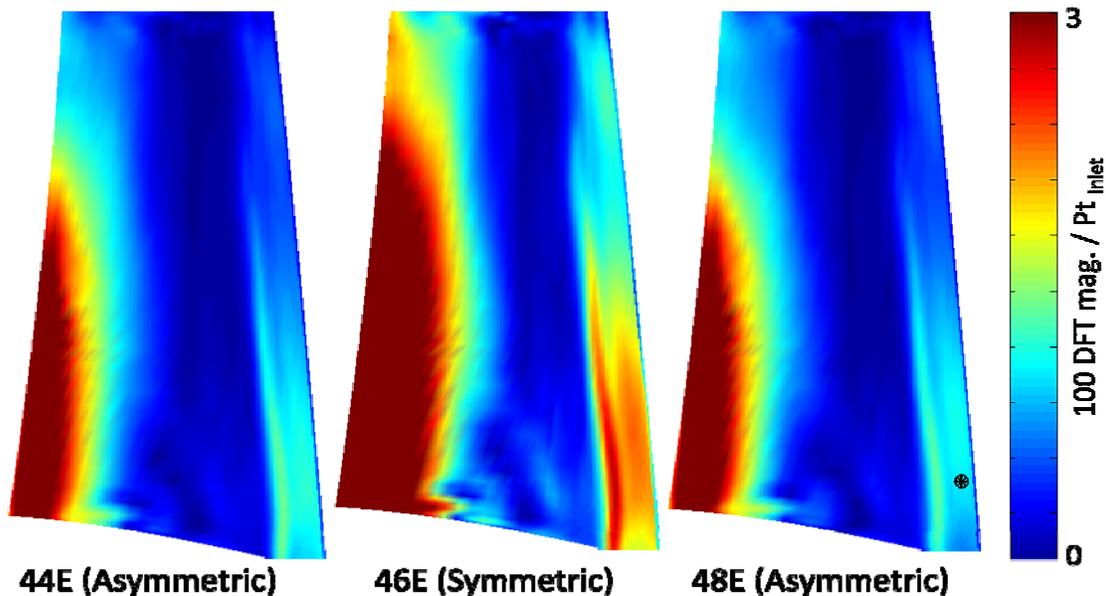

Fig. 4.10. Asymmetric vane-spacing reduces the magnitude of blade unsteady pressures at twice vane passing over the entire region of the blade that is affected by shock reflection.

4.6   Vane-to-Vane Clocking

In airfoil clocking the position between successive blade and/or vane rows is intentionally shifted in the circumferential direction. This relative difference in circumferential position is usually intended to control the location of airfoil wakes as they propagate downstream through successive airfoil rows in order to achieve an aero-performance benefit. Huber et al. [37] were the first to demonstrate a variation in turbine efficiency with airfoil indexing in an experimental program with analytical support [38] that focused on the turbo-pump of the Space Shuttle Main Engine (SSME). Since that time, many others have replicated the work for other turbomachines [e.g. 39, 40, 84, and 85], and the concept has also inspired the clocking of combustor-nozzle hot streaks to achieve improved component durability [41-44]. However, it is also possible that the relative phase of upstream- and downstream-propagating disturbances could act to alter the unsteady load on a turbine blade that is located between clocked vane rows [86, 87], and one can envisage this as either a detriment or a benefit to the durability of the design.

The HIT RT was designed with equal upstream and downstream airfoil counts to allow for airfoil clocking investigations. One can index the downstream vane relative to the inlet guide vane over a number of circumferential positions, and the design clocking position is shown in Fig. 4.11 along with two of the off-design locations analyzed here. In the figure, the view is aft-looking-forward and the instantaneous static pressure field on the surfaces of the airfoils is plotted with the 2V suction side clearly visible. Relative to the HIT RT blade row there is an upstream-propagating potential field from the downstream vane and downstream-propagating vortical disturbances from the inlet guide vane. The flowfield is further complicated by the upstream propagation of shock reflections from the downstream vane. So, one might expect dramatic effects of clocking on both predicted aero-performance and unsteady blade loads.
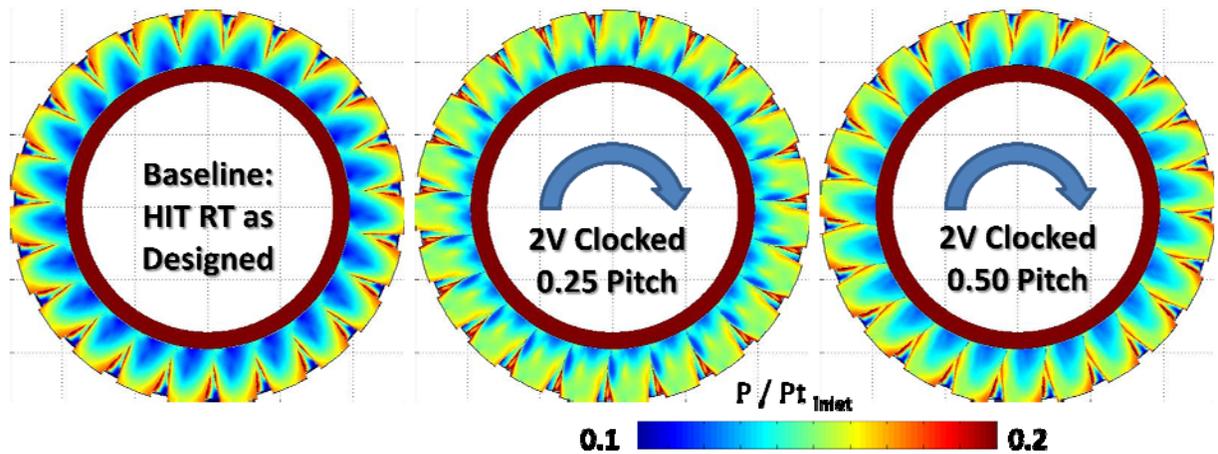

Fig. 4.11. Instantaneous static pressure on the airfoils of the HIT RT at three clocking positions. The view is aft-looking-forward.

Figure 4.12 is a plot of predicted aero-performance variation as a function of clocking position. The performance is presented on a delta basis relative to the predicted efficiency at the design clocking position. One notes that the turbine is designed at near the optimum indexing between rows in terms of aero-performance. Also, the predicted peak-to-peak variation in performance is of order 0.1%. This is much less than that typically reported in the literature from experiments [37, 84]. However, it is well in keeping with the range typically predicted to occur [38, 39].
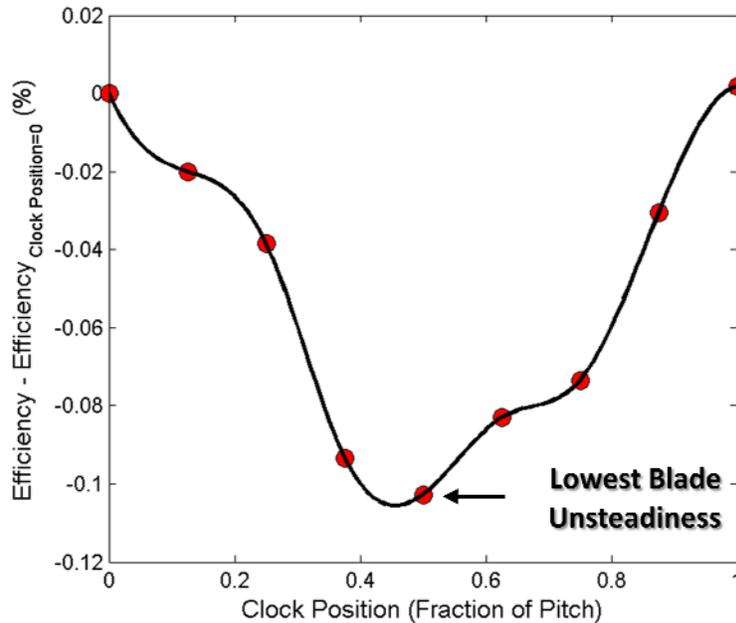
Fig. 4.12. The variation of aero-performance with clocking position for the HIT RT. The turbine is at near-peak performance as designed. The location of minimum performance is coincident with that for minimum blade/downstream vane interaction.

Clocking of the downstream vane with respect to the nozzle guide vane does affect the predicted unsteadiness on the blade row markedly both in terms of DFT magnitude and phase. Fig. 4.13 is a set of DFT magnitude distributions at twice vane passing frequency for the clocking locations illustrated in Fig. 4.11. At a clocking position of one-half pitch relative to the design intent, the effect of shock reflections on the unsteady pressure on the blade suction side downstream of the cross-channel shock is minimized. This corresponds to the location of lowest aero-performance plotted in Fig. 4.12. So, for this turbine the selection of clocking location would become ultimately a design choice, depending on whether the analyst intends to achieve high performance or reduced stress at some crossing on the Campbell diagram. This illustrates the need to perform time-resolved unsteady analysis during the design cycle of a turbine.
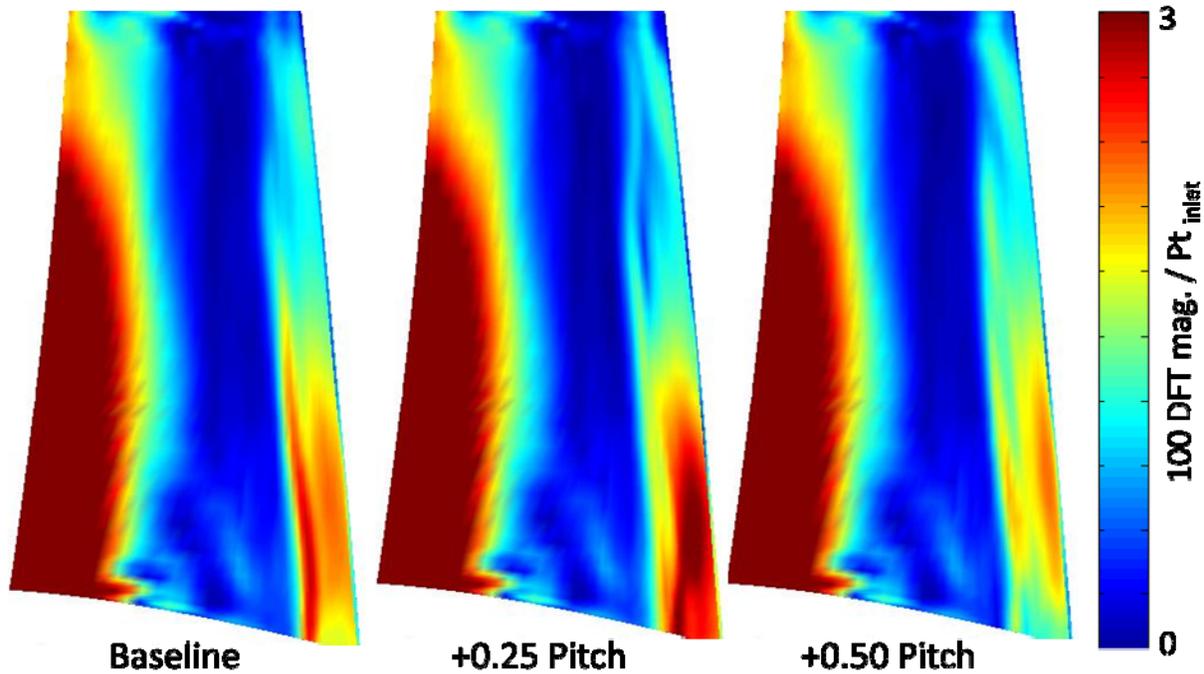
Fig. 4.13. DFT magnitudes as twice vane passing on the blade suction side for the three indexing levels shown in Fig. 4.11. Minimum interaction due to shock reflections occurs at a clocking location of one-half pitch.

The clocking location of the downstream vane also has a dramatic effect on the phase of blade unsteadiness. Figure 4.14 is a plot of phase variation versus span at 95% chord on the blade suction side for nine levels of indexing including the design intent. While the peak-to-peak variation in phase over the span does not change appreciably with clocking location, the mean level does change markedly. Again, resonant stresses arise due to high levels of unsteady pressure variations that are in phase with oscillations of the blade, so full high cycle fatigue predictions are necessary during design. However, it is quite clear from the analyses performed that clocking has a large effect on aerodynamic forcing functions, and this characteristic of airfoil indexing is potentially of more significance to the success of a design than the effect on aero-performance.

5.   Summary

In this lecture, it was argued that aerodynamic designers must gain confidence in their predictions of time-varying loads on rotating airfoils prior to any attempt to mitigate unsteady interaction between airfoils rows. This confidence is achievable through rigorous checks on the convergence of simulations coupled with judicious post-processing of predicted flowfields

with respect to the requirements and limitations of resonant-stress evaluation systems. Further, the usefulness of proactive validation and verification exercises targeted at design-level predictions of airfoil unsteady pressures in relevant physical environments was discussed. It is possible to leverage the lessons learned from such code validation studies directly in the development of new turbomachines. It was also shown that it is possible to assess several possible design solutions to a resonant-stress problem quickly by performing the most rigorous unsteady analyses possible given available manpower and computational resources. From the six examples of turbine-component re-design presented here it is clear that one can find simple and effective means for mitigating unsteady interaction during the design cycle. Further, each of the methods presented is suitable for implementation in design optimization systems.
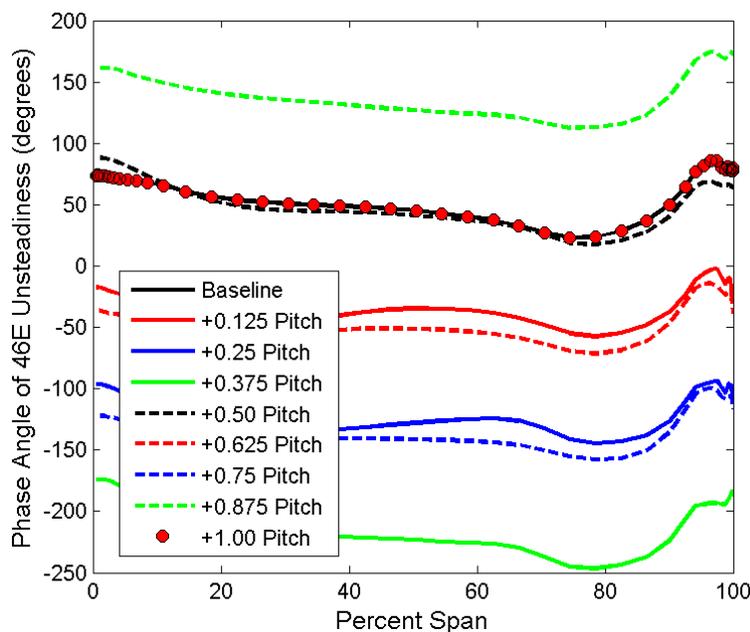
Fig. 4.14. DFT phase angle variation at twice vane passing as a function of span at 95% chord on the blade suction side. Nine different clocking locations are shown, and the effect of indexing on mean phase over the span is dramatic.

6. Acknowledgments

7.   Nomenclature

Latin

A	DFT magnitude
b_x	airfoil axial chord (cm)
CCF	Cross-Correlation Coefficient
DFT	Discrete Fourier Transform
E	Engine order = frequency / (rpm / 60)
f	Membership grade in a fuzzy set
k	Integer multiple of sampling frequency
L	Number of lags
M	Mach number
n_{af}	number of airfoils in a given row
N	wheel speed (rpm)
N	Number of samples per periodic cycle
n	Integer multiple of sampling interval
P	Fourier component of static pressure signal
$P_{t,in}$	Inlet total pressure (M Pa)
p	Static pressure (M Pa)
PS	pressure side
PSD	Power Spectral Density
r	radial distance (cm, in)
Re	Reynolds number based on axial chord
SS	suction side
T_t	Total temperature (K)
Tu	turbulence intensity (%)
U	rotor tangential velocity (m/s)
x	axial distance (cm, in)
y^+	non-dimensional distance (i.e. law-of-the-wall variable)
1B	first blade
1V	first vane
1VPF	first vane passing-frequency (fundamental) = $(n_{af}\ N) / 60$
2V	second vane

Greek

Δf	Spectral resolution (Hz) of a signal = 1 / (N Δt)
Δt	Sampling rate, temporal resolution of a signal (s)
Φ	DFT phase angle (radians, degrees)
ω	Circular frequency (radians / s)

Subscripts / Superscript

A	Fuzzy set for convergence of DFT amplitude
C	Fuzzy set for overall convergence
M	Fuzzy set for time-mean convergence
P	Fuzzy set for fraction of overall signal power
S	Fuzzy set for convergence of overall signal shape
Φ	Fuzzy set for convergence of DFT phase angle
'	Fluctuating component

8. References

[1] Tyler, J. M. and Sofrin, T. G., 1970, "Axial Flow Compressor Noise Studies," SAE Transactions, Vol. 70, pp. 309-332.

[2] Rangwalla, A. A. and Rai, M. M., 1993, "A Numerical Analysis of Tonal Acoustics in Rotor-Stator Interactions," Journal of Fluids and Structures, Vol. 7, pp. 611-637.

[3] Dring, R. P., Joslyn, H. D., Hardin, L. W., and Wagner, J. H., 1982, "Turbine Rotor-Stator Interaction , ASME Journal of Engineering for Power," Vol. 104, pp. 729-742.

[4] Dunn, M. G. and Haldeman, C. W., Jr., 1995, "Phase-Resolved Surface Pressure and Heat-Transfer Measurements on the Blade of a Two-Stage Turbine," ASME Journal of Fluids Engineering, Vol. 117, pp. 653-658.

[5] Rai, M. M., 1987, "Navier-Stokes Simulations of Rotor-Stator Interaction Using Patched and Overlaid Grids," AIAA Journal of Propulsion and Power, Vol. 3, pp. 387-396.

[6] Giles, M. B., 1990, "Stator/Rotor Interaction in a Transonic Turbine," AIAA Journal of Propulsion and Power, Vol. 6, pp. 621-627.

[7] Greitzer, E. M., Tan, C. S., Wisler, D. C., Adamczyk, J. J., and Strazisar, A. J., 1994. Unsteady Flows in Turbomachines: Where's the Beef?," Unsteady Flows in Aeropropulsion, ASME AD-Vol. 40, pp. 1-11.

[8] Sharma, O. P., Pickett, G.F., and Ni, R.H., 1992, "Assessment of Unsteady Flows in Turbines," ASME Journal of Turbomachinery, Vol. 114, pp. 79-90.

[9]   Paniagua, G. and Denos, R., 2007, "Unsteadiness in HP Turbines," in Advances in Turbomachinery Aero-Thermo-Mechanical Design Analysis, VKI Lecture Series 2007-02.

[10]   Dunn, M. G., 2001, "Convective Heat Transfer and Aerodynamics in Axial Flow Turbines," ASME Journal of Turbomachinery, Vol. 123, pp. 637-686.

[11]   Adamczyk, J. J., 2000, "Aerodynamic Analysis of Multi-Stage Turbomachinery Flows in Support of Aerodynamic Design," ASME Journal of Turbomachinery, Vol. 122, pp. 189-217.

[12]   Ni, R.H., 1999, "Advanced Modeling Techniques for New Commercial Engines," XIV ISOABE Conference, Florence, Italy, 5-10 September.

[13]   Hilbert, G. R., Ni, R. H., and Takahashi, R. K., 1997, "Forced-Response Prediction of Gas Turbine Rotor Blades," Analysis and Design Issues for Modern Aerospace Vehicles, Proceedings of the Symposia, ASME International Mechanical Engineering Congress and Exposition, Dallas, TX, 16-21 Nov., pp. 491-498.

[14]   Green, J. S. and Marshall, J. G., 1999, "Forced Response Prediction within the Design Cycle," IMechE Conference Transactions 1999-1A, pp. 377-391.

[15]   Chiang, H. D. and Kielb, R. E., 1993, "An Analysis System for Blade Forced Response," ASME Journal of Turbomachinery, Vol. 115, pp. 762-770

[16]   Seinturier, E., Lombard, J-P., Dumas, M., Dupont, C., Sharma, V., Dupeux, J., 2004, "Forced-Response Methodology for the Design of HP Compressors Bladed Disks," ASME Paper No. GT2004-53372.

[17]   Montgomery, M., Tartibi, M., Eulitz, F., and Schmitt, S., 2005, "Application of Unsteady Aerodynamics and Aeroelasticity in Heavy Duty Gas Turbines," ASME Paper No. GT2005-68813.

[18]   Filsinger, D., Frank, Ch., and Schafer, O., 2005, "Practical Use of Unsteady CFD and FEM Forced Response Calculation in the Design of Axial Turbocharger Turbines," ASME Paper No. GT2005-68439.

[19]   Sipatov, A. M., Gladisheva, N. V., Avgustinovich, V. G., and Povishev, I. A., 2007, "Tools for Estimating Resonant Stresses in Turbine Blades," ASME Paper No. GT2007-27196.

[20]   Jones, T. V., Schultz, D. L., and Henley, A. D., 1973, "On the Flow in an Isentropic Light Piston Tunnel," ARC Report No. 34217, U.K.

[21]   Dunn, M. G., Moller, J. C., and Steele, R. C., 1989, "Operating Point Verification for a Large Shock Tunnel Test Facility," Calspan Report No. WRDC-TR-2027.

[22]   Rao, K. V., Delaney, R.A., and Dunn, M.G., 1994, "Vane-Blade Interaction in a Transonic Turbine, Part 1: Aerodynamics," ASME Journal of Propulsion and Power, Vol. 10, No. 3, pp. 305-311.

[23]   Busby, J. A., Davis, R. L., Dorney, D. J., Dunn, M. G., Haldeman, C. W., Jr., Abhari, R. S., Venable, B. L., and Delaney, R. A., 1998. Influence of Vane-Blade Spacing on Transonic Turbine Stage Aerodynamics, Part II: Time-Resolved Data and Analysis, ASME Paper No. 98-GT-482.

[24] Hilditch, M. A., Smith, G. C., and Singh, U. K., 1998, "Unsteady Flow in a Single Stage Turbine," ASME Paper No. 98-GT-531.

[25] Haldeman, C. W., Dunn, M. G., Abhari, R. S., Johnson, P. D., and Montesdeoca, X. A., 2000, "Experimental and Computational Investigation of the Time-Averaged and Time-Resolved Pressure Loading on a Vaneless Counter-Rotating Turbine," ASME Paper No. 2000-GT-0445.

[26] Kost, F., Hummel, F., and Tiedemann, M., 2000, "Investigation of the Unsteady Rotor Flow in a Single-Stage HP Turbine Stage," ASME Paper No. 2000-GT-0432.

[27] Laumert, B., Martensson, H, and Fransson, T. H., 2002, "Investigation of Unsteady Aerodynamic Blade Excitation Mechanisms in a Transonic Turbine Stages," ASME Paper No. GT2002-30450.

[28] Bakhle, M. A., Liu, J. S., Panovsky, J., Keith, T. G., and Mehmed, O., 2002, "Calculation and Correlation of the Unsteady Flowfield in a High Pressure Turbine," ASME Paper No. GT2002-30322.

[29] Kielb, J. J., Abhari, R. S., and Dunn, M. G., 2001, "Experimental and Numerical Study of Forced Response in a Full-Scale Rotating Turbine," ASME Paper No. 2001-GT-0263.

[30] Hennings, H. and Elliot, R., 2002, "Forced Response Experiments in a High Pressure Turbine Stage," ASME Paper No. GT2002-30453.

[31] Kielb, J. J. and Abhari, R. S., 2001, "Experimental Study of Aerodynamic and Structural Damping in a Full-Scale Rotating Turbine," ASME Paper No. 2001-GT-0263.

[32] Jennions, I. K. and Adamczyk, J. J., 1997, "Evaluation of the Interaction Losses in a Transonic Turbine HP Rotor / LP Vane Configuration," ASME Journal of Turbomachinery, Vol. 119, pp. 68-75.

[33] Ni, R. H., 1982, "A Multiple-Grid Scheme for Solving the Euler Equations," AIAA Journal, Vol. 20, No. 11, pp. 1565-1571.

[34] Ni, R. H. and Bogoian, J. C., 1989, "Prediction of 3-D Multistage Turbine Flow Field Using a Multiple-Grid Euler Solver," AIAA Paper No. 89-0203.

[35] Davis, R. L., Shang, T., Buteau, J., and Ni, R. H., 1996, "Prediction of 3-D Unsteady Flow in Multi-Stage Turbomachinery Using an Implicit Dual Time-Step Approach," AIAA Paper No. 96-2565.

[36] Weaver, M. M., Manwaring, S. R., Abhari, R. S., Dunn, M. G., Salay, M. J., Frey, K. K., and Heidegger, N., 2000, "Forcing Function Measurements and Predictions of a Transonic Vaneless Counter-Rotating Turbine," ASME Paper No. 2000-GT-0375.

[37] Huber, F., Johnson, P. D., Sharma, O. P., Staubach, J. B., and Gaddis, S. W., 1996, "Performance Improvement Through Indexing of Turbine Airfoils: Part 1-Experimental Investigation," ASME Journal of Turbomachinery, Vol. 118, pp. 630-635.

[38] Griffin, L. M., Huber, F. W., and Sharma, O. P., 1996, "Performance Improvement Through Indexing of Turbine Airfoils: Part 2- Numerical Simulation," ASME Journal of Turbomachinery, Vol. 118, pp. 636-642.

[39] Dorney, D. J., and Sharma, O. P., 1996, "A Study of Turbine Performance Increases Through Clocking," AIAA Paper No. 96-2816.

[40] Haldeman, C. W., Dunn, M. G., Barter, J. W., Green, B. R., and Bergholz, R. F., 2005, "Experimental Investigation of Vane Clocking in a One and 1/2 Stage High Pressure Turbine, ASME Journal of Turbomachinery, Vol. 127, pp. 512-521 (Also ASME Paper No. GT2004-5347).

[41] Shang, T. and Epstein, A. H., 1997, "Analysis of Hot Streak Effects on Turbine Rotor Heat Load," ASME Journal of Turbomachinery, Vol. 119, No. 3, pp. 544-553..

[42] Takahashi, R. K., Ni, R. H., Sharma, O. P., and Staubach, J. B., 1996, "Effects of Hot Streak Indexing in a 1-1/2 Stage Turbine," AIAA Paper No. 96-2796.

[43] Dorney, D. J., and Gundy-Burlet, K., 2000, "Hot-Streak Clocking Effects in a 1-1/2 Stage Turbine," AIAA Journal of Propulsion and Power, Vol. 12, No. 3, pp. 619-620.

[44] He, L., Menshikova, V., and Haller, B. R., 2004, "Influence of Hot Streak Circumferential Length-Scale in a Transonic Turbine Stage," ASME Paper No. GT2004-53370.

[45] Munk, M. and Prim, R., 1947, "On the Multiplicity of Steady Gas Flows Having the Same Streamline Pattern," Proceedings of the National Academy of Sciences, Vol. 33, pp. 137-141.

[46] Roache, P. J., 1998, Verification and Validation in Computational Science and Engineering, Hermosa Publishers, Albuquerque, NM, USA.

[47] Gokaltun, S., Skudarnov, P. V., and Lin, C-X., 2005, "Verification and Validation of CFD Simulation of Pulsating Laminar Flow in a Straight Pipe," AIAA Paper No. 2005-4863.

[48] Guide for the Verification and Validation of Computational Fluid Dynamics Simulations, AIAA Policy Paper G-077-1998, AIAA, Reston, VA, USA.

[49] Freitas, C. J., 1993, "Editorial Policy Statement on the Control of Numerical Accuracy," ASME *Journal of Fluids Engineering*, Vol. 115, No. 2, pp. 339.

[50] Laumert, B., Martensson, H, and Fransson, T. H., 2002, "Investigation of Unsteady Aerodynamic Blade Excitation Mechanisms in a Transonic Turbine Stage, Part I: Phenomenological Identification and Classification," ASME Journal of Turbomachinery, Vol. 124, pp. 410-418 (Also ASME Paper No. 2001-GT-0258).

[51] Ahmed, M. H. and Barber, T. J., 2005, "Fast Fourier Transform Convergence Criterion for Numerical Simulations of Periodic Fluid Flows," AIAA Journal, Vol. 43, No. 5, pp. 1042-1052.

[52] Staubach, J. B., 2003, "Multidisciplinary Design Optimization, MDO, the Next Frontier of CAD/CAE in the Design of Aircraft Propulsion Systems," AIAA Paper No. 2003-2803.

[53]   Shahpar, S. and Lapworth, L., 2003, "PADRAM: Parametric Design and Rapid Meshing for Turbomachinery Optimization," ASME Paper No. GT2003-38698.

[54]   Shahpar, S., Giacche, D., and Lapworth, L., 2003, "Multi-Objective Design and Optimization of Bypass Outlet-Guide Vanes," ASME Paper No. GT2003-38700.

[55]   Ifeachor, E. C. and Jervis, B. W., 1996, Digital Signal Processing, Addison-Wesley, New York.

[56]   Signal Processing Toolbox User's Guide, Version 5, 2000, The Mathworks, Natick, MA.

[57]   Jocker, M., and Fransson, T. H., 2002, "Mode Shape Sensitivity of the High Pressure Turbine Rotor Excitation Due to Upstream Stators," ASME Paper No. GT2002-30452.

[58]   Klir, G.J., St. Clair, U.H., and Yuan, B., 1997, Fuzzy Set Theory: Foundations and Applications, Prentice Hall PTR, Upper Saddle River, NJ.

[59]   Clark, J.P. and Yuan, B., 1998, "Using Fuzzy Logic to Detect Turbulent/Non-Turbulent Interfaces in an Intermittent Flow," Intelligent Automation and Control, Vol. 6, pp. 113-118, TSI Press, Albuquerque, NM

[60]   Zimmermann, H. J. 1990, Fuzzy Set Theory and Its Applications, Second Edition, Kluwer, Boston, MA.

[61]   Klir, G. J. and Yuan, B., 1995, Fuzzy Sets and Fuzzy Logic: Theory and Applications, Prentice Hall PTR, Upper Saddle River, NJ.

[62]   Johnson, P. D., 2005, "Consortium Turbine Research Rig, Aerothermal and Mechanical Design," AFRL Technical Report AFRL-PR-WP-TR-2005-2157.

[63]   Dorney, D. J. and Davis, R. L., 1992, "Navier-Stokes Analysis of Turbine Blade Heat Transfer and Performance," ASME Journal of Turbomachinery, Vol. 114, pp. 795-806.

[64]   Rai, M. M. and Madavan, N. K., 1990, "Multi-Airfoil Navier-Stokes Simulations of Turbine Rotor-Stator Interaction," ASME Journal of Turbomachinery, Vol. 112, pp. 377-384.

[65]   Polanka, M.D., Hoying, D.A., Meininger, M., and MacArthur, C.D., 2003, "Turbine Tip and BOAS Heat Transfer and Loading, Part A: Parameter Effects Including Reynolds Number, Pressure Ratio and Gas to Metal Temperature Ratio", ASME Journal of Turbomachinery, Vol. 125, pp. 97-106.

[66]   Clark, J. P., Polanka, M. D., Meininger, M., and Praisner, T. J., 2006, "Validation of Heat-Flux Predictions on the Outer Air Seal of a Transonic Turbine Blade," ASME Journal of Turbomachinery, Vol. 128, pp. 589-595.

[67]   Kielb, R. E., Barter, J. W., Thomas, J. P., and Hall, K. C., 2003, "Blade Excitation by Aerodynamic Instabilities – A Compressor Blade Study," ASME Paper No. GT2003-38634.

[68]   Sanders, A. J., 2005, "Non-Synchronous Vibration (NSV) Due to a Flow-Induced Aerodynamic Instability in a Composite Fan Stator," ASME Journal of Turbomachinery, Vol. 127, pp. 412-421 (Also ASME Paper No. GT2004-53492).

[69] Doorly, D. J. and Oldfield, M. L. G., 1985, "Simulation of the Effects of Shock Wave Passing on a Turbine Rotor Blade," ASME Journal of Engineering for Gas Turbines and Power, Vol. 107, pp. 998-1006.

[70] Clark, J. P., Aggarwala, A. S., Velonis, M. A., Magge, S. S., and Price, F. R., 2002, "Using CFD to Reduce Resonant Stresses on a Single-Stage, High-Pressure Turbine Blade," ASME Paper No.GT2002-30320.

[71] Clark, J. P., Stetson, G. M., Magge, S. S., Dunn, M. G., and Haldeman, C. W., 2000, "The Effect of Airfoil Scaling on the Unsteady Aerodynamics of a 1 and 1/2 Stage Transonic Turbine and a Comparison with Experimental Results", ASME Paper No. 2000-GT-446.

[72] Ni, R. H., Humber, W., Fan, G., Johnson, P. D., Downs, J., Clark, J. P., and Koch, P. J., 2011, "Conjugate Heat Transfer Analysis of a Film-Cooled Turbine Vane," ASME Paper No. GT2011-45920.

[73] Wilcox, D. C., 2003, *Turbulence Modeling for CFD*, Second Edition, DCW Industries, Inc., La Cañada, CA, USA.

[74] Lax, P. D., and Wendroff, B., 1964, "Difference Schemes for Hyperbolic Equations with High Order Accuracy," Communications on Pure and Applied Mechanics, Vol. 17, pp. 381-398.

[75] Clark, J. P., 2010, "Shock Cancellation Mechanism for the Control of Unsteady Interaction in Contra-Rotating High- and Low-Pressure Turbines," U.S. Patent Pending.

[76] Joly, M., Verstraete, T., and Paniagua, G., 2010, "Attenuation of Vane Distortion in a Transonic Turbine Using Optimization Strategies, Part I – Methodology," ASME Paper No. GT2010-22370.

[77] Joly, M., Paniagua, G., and Verstraete, T., 2010, "Attenuation of Vane Distortion in a Transonic Turbine Using Optimization Strategies, Part II – Optimization," ASME Paper No. GT2010-22371.

[78] Paniagua G., Saracoglu B., Yasa T., Salvadori S., Martelli F., 2011, "Modulation of Vane Shocks with Pulsating Coolant Flows". To be presented at the 47th Joint Propulsion Conference, San Diego, CA, USA.

[79] Paniagua G. and Saracoglu B., 2010, "Pulsating trailing edge jet for shockwave alleviation," European Patent Application No. PCT/EP2010/057864.

[80] Kemp, R. H., Hirschberg, M. H., and Morgan, W. C., 1958, "Theoretical and Experimental Analysis of the Reduction of Rotor Blade Vibration in Turbomachinery Through the Use of Modified Stator Vane Spacing," NACA TN 4373.

[81] Kaneko, Y., Mori, K., and Okui, H., 2004, "Study on the Effect of Asymmetric Vane Spacing on Vibratory Stress of Blade," ASME Paper No. GT2004-53023.

[82] Miyakozawa, T., Kielb, R. E., and Hall, K. C., 2009, "The Effects of Aerodynamic Asymmetric Perturbations on Forced Response of Bladed Discs," ASME Journal of Turbomachinery, Vol. 131, pp. 041008-1-041008-8.

[83] Ekici, K., Kielb, R. E., and Hall, K. C., 2010, "Aerodynamic Asymmetry Analysis of Unsteady Flows in Turbomachinery," ASME Journal of Turbomachinery, Vol. 132, pp. 011006-1-011006-11.

[84] Jouini, D. B. M., Little, D., Bancalari, E., Dunn, M. G., Haldeman, C. W., and Johnson, P. D., 2003, "Experimental Investigation of Airfoil Wake Clocking Impacts on Aerodynamic Performance in a Two Stage Turbine Test Rig," ASME Paper No. GT2003-38872.

[85] Haldeman, C. W., Dunn, M. G., Barter, J. W., Green, B. R., and Bergholz, R. F., 2005, "Experimental Investigation of Vane Clocking in a One and One-Half Stage High Pressure Turbine," ASME Journal of Turbomachinery, Vol. 127, pp. 512-521.

[86] Haldeman, C. W., Krumanaker, M. L., and Dunn, M. G., 2003, "Influence of Clocking and Vane/Blade Spacing on the Unsteady Surface Pressure Loading for a Modern Stage and One-Half Transonic Turbine," ASME Paper No. GT2003-38724.

[87] Schennach, O., Pecnik, R., Paradiso, B., Göttlich, E., Marn, A., and Woisetschläger, J., 2007, "The Effect of Vane Clocking on the Unsteady Flowfield in a One and a Half Stage Transonic Turbine," ASME Paper No. GT2007-27848.

[88] Clark, J. P., and Grover, E. A., 2007, "Assessing Convergence in Predictions of Periodic-Unsteady Flowfields," ASME Journal of Turbomachinery, Vol. 129, pp. 740-749.